Design and Characterization of Integrin α4β1-Specific DNA Aptamer Conjugates for Cancer Targeting Applications

Jai Raman

A thesis submitted in partial fulfillment of the requirements for the degree of:

Master of Science in Bioengineering

University of Washington

2022

Committee:

Suzie Pun

Hao Yuan Kueh

Program Authorized to Offer Degree:

Bioengineering

University of Washington

Abstract

Design and Characterization of Integrin α4β1-Specific DNA Aptamer Conjugates for Cancer Targeting Applications

Jai Raman

Chair of the Supervisory Committee:

Suzie Pun, Ph.D.

Cancer can exert a burdensome toll on all in its grasp, causing physical as well as psychological distress. Therapies currently in use to treat cancer either carry a variety of unpleasant side-effects or are prohibitively expensive. Therapies using active antigen targeting strategies present one solution. While antibody intermediates have been used in this strategy, DNA aptamers surprisingly have yet to see this application. Owing to their many advantages as safe, low cost, high-affinity targeting ligands, we hypothesize that cancer-specific DNA aptamers can serve as powerful, cost-effective, and safe tools for a variety of cancer targeting applications. Despite their favorable properties on paper however, aptamers experience three major challenges in vivo. Aptamers are readily degraded by nucleases in blood serum, assume different conformations at body temperature compared to 4C, and are subject to rapid renal filtration due to their small size. Fortunately, there are various strategies that can be employed to mitigate the aforementioned issues. Through rational chemical modification and conjugation of aptamers to various moieties, it is possible to improve the in vivo pharmacokinetics of aptamers. Thus, this project explores the characterization, modification, and potential application of HR7A1, a cancer selective integrin α4β1-specific aptamer. The results of this project will better inform the development of more aptamer-based targeted therapies to expand the accessibility of precision medicine to all patients.

Introduction

Cancer is a significant public health problem around the world, and the second leading cause of death in the United States. Despite their general success, therapies currently in use to treat cancer cause numerous detrimental side-effects. Existing chemotherapeutic drugs are toxic to all cells, attacking both cancer and healthy cells, and untargeted radiation therapy suffers from a similar lack of specificity. And while surgery is a powerful tool for removing large, localized tumors, cancer metastasis severely undermines the effectiveness of surgical procedures. As such, there is a pressing need for a safe, effective treatment option that can cover the weaknesses of current therapies while circumventing the several associated side-effects.

Targeted therapies–specifically, therapies with active targeting–represent one promising alternative treatment route. "Active-targeting" is a term used to describe specific ligand–receptor interactions between drugs or drug carriers and target cells [1]. For oncology indications, antigen-specific ligands can be engineered to block receptor function on cancer cells, flag cells for destruction by the immune system, or carry and deliver drug payloads to cells of the tumor microenvironment [2]. The effectiveness of such therapies relies on targeting cancer cells with high specificity while minimizing on-target, off-tumor side effects on healthy tissues. To date, monoclonal antibodies have primarily seen this application, with over 100 therapeutic antibody drugs approved by the FDA in the last 35 years [3]. However, antibody production is an expensive process, and antibodies further stymied by their low shelf-life and high batch-to-batch variation. This results in a prohibitively expensive treatment option, with the average monoclonal antibody therapy exceeding $100,000 in 2018 [4]. Accordingly, less expensive targeting ligands are required to make this strategy more cost-effective.

Aptamers, single-stranded oligonucleotides that adopt sequence-specific secondary structures and bind specific proteins, are amenable to addressing these highlighted issues [5]. Aptamers can match the excellent binding affinity of antibodies and are small in size (10-30 kDa), allowing for enhanced tissue penetration. Importantly, aptamers are synthetically produced, enabling inexpensive production and high control over chemical modifications. Aptamers also have a near-unlimited shelf life and exhibit little immunogenicity. However, the current lack of aptamer therapeutics on the market is no coincidence. For all their benefits on paper, aptamers have yet to translate their success from the lab to the bedside as a revolutionary new treatment option. This can be primarily attributed three reasons: their low serum stability, propensity for changing conformation (resulting in a reduction of binding) at in vivo temperatures, and their small, anionic nature, which results in rapid renal clearance [6].

These issues are well-known in the field, and researchers have developed a wide array of techniques to overcome these challenges. Ni et al. explored various chemical modifications to DNA aptamers, discussing the merits of 3'-inverted dT modification, 2'-O-Methylation, locked nucleic acids (LNA), and phosphorothioate bonds as potential solutions [7]. Zeng et al. demonstrated the viability of an aptamer-dye conjugate for specific and sensitive tumor imaging system [8]. The aptamer was conjugated to the dye via amine- NHS-ester chemistry and provided the aptamer with enhanced serum stability compared to RNA aptamer probes of similar specificity. The same CD30 aptamer was further studied for in vivo applications, owing to the antigen's high expression in Hodgkin's lymphoma and anaplastic large cell lymphoma, demonstrating the viability of aptamers in immunotherapy through the use of optimal chemical modifications to increase serum stability [9].

Current targeted drug delivery systems rely on blood circulation and extravasation to reach the site of disease [10]. For maximum therapeutic effect, the drug must be retained and distributed intratumorally. However, the average diameter of aptamers (10-30 kD) is less than 5 nm; due to this size, aptamers lack the circulation half-lives of larger molecules [11]. Despite their small size causing rapid renal filtration, the in vivo pharmacokinetic profile of aptamers can be improved through rational chemical modification and conjugation. One of the primary methods of overcoming kidney filtration and extending circulating half-life is to conjugate aptamers to a bulky moiety. This can include groups such as such as cholesterol, proteins, liposomes, nanomaterials, or high molecular weight PEG [12]. Macugen, the only FDA-approved therapeutic aptamer to date, is formulated with a 40 kD branched PEG conjugate and has a circulation half-life of 9.3h after IV injection [13]. Aptamers can also be multimerized to create a multivalent molecule above the renal glomerulus molecular weight cutoff (30–50 kD) [14]. Many of these conjugate groups can also provide additional shielding from nucleases in blood sera, helping further mitigate aptamer degradation.

Systematic evolution of ligands by exponential enrichment (SELEX) is currently the gold-standard protocol for discovering high-affinity aptamers for use in a variety of technologies, including targeted therapies. SELEX comprises an iterative selection process, using sequential positive and negative selection to identify high-affinity binders from a naïve aptamer library that can contain up to 10^{15} unique aptamer sequences. In positive selection rounds, aptamers that bind to the target cell type are isolated and enriched, while in negative selection, aptamers that bind to control cells are removed while non-binders are enriched. After several rounds of SELEX, the aptamers with high presence in the resulting pool are sequenced to reveal their structures.

This project focuses specifically on an aptamer discovered in the Pun laboratory through a SELEX process targeting H9 cells, a T-leukemia cell line. The aptamer with the highest presence after seven rounds of positive and negative selection was called HR7A1 (**H**9 **R**ound **7** **A**ptamer **1)**. The 88 base-pair HR7A1 aptamer was first truncated to remove the 33 base-pair constant region that did not contribute to the active conformation and binding properties of the aptamer (Figure 1). Smaller aptamers carry several advantages, such as increased tumor penetration and lower synthesis costs. Thus, the resulting 55bp aptamer, HR7A1 Trunc1, was further shortened by removing smaller toehold structures that were suspected to not contribute to aptamer binding. The resulting 42 base-pair aptamer was called HR7A1 Trunc2 and is the smallest aptamer produced by our lab thus far.

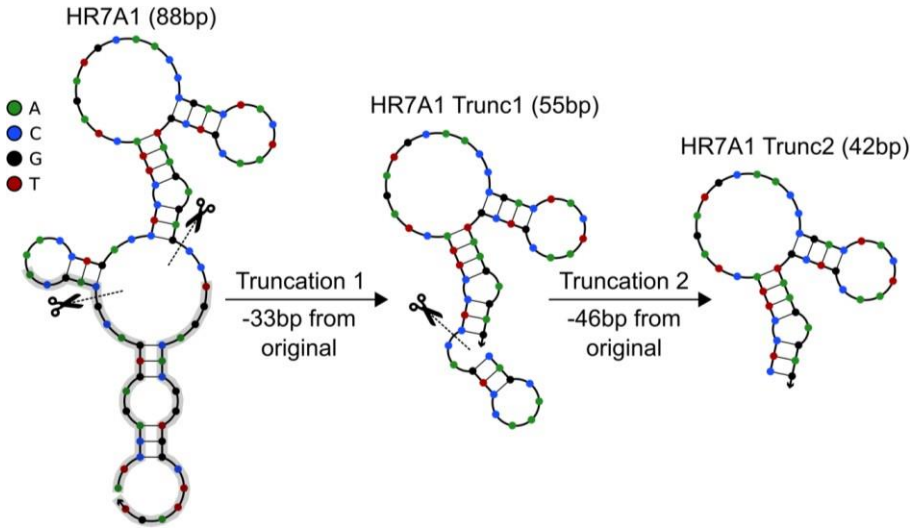

Figure 1. NUPACK predicted structures of HR7A1, HR7A1 Trunc1, and HR7A1 Trunc2 at 4C

Preliminary binding studies revealed the aptamer's cancer selective properties (Figure S1), while membrane pull down assays indicated the integrin α4β1 as a potential receptor target. Integrin α4β1, also known as VLA-4, is a heterodimer consisting of two subunits: CD49d (α4) and CD29 (β1). Like all integrins, the role of α4β1 is ensure that cells are properly connected to and can receive signals from the extracellular matrix (ECM). In addition, α4β1 also participates in

interactions between antigen presenting cells and lymphocytes, regulates immune cell trafficking to sites of inflammation, and mobilizes immature progenitor cells in the bone marrow [15]. Most importantly, the overexpression of the α4β1 receptor has been linked to the progression and persistence of numerous types of leukemia and lymphoma, providing the foundation for this project [16].

The goals of this project were manifold. First, to produce a thorough characterization and construct a comprehensive binding profile of the HR7A1 aptamer and its truncated variants. Secondly, to evaluate and potentially improve the serum stability of the aptamer. Third, to assess the conformational stability of the aptamer at 37C and design modifications to the aptamer to raise thermal stability. Last, to develop aptamer-conjugate constructs to increase the circulation half-life of the aptamer. The overarching objective of this study is to produce a robust aptamer capable of both therapeutic and diagnostic applications as an inexpensive yet alternative to existing technologies.

Results and Discussion

I. Aptamer Characterization

The first step following the discovery of an aptamer is its characterization, to full elucidate the target receptor, binding affinity, and binding kinetics. Although preliminary membrane pull-down assays revealed integrin α4β1 as the target receptor of the aptamer, it was unknown whether the aptamer bound to a specific subunit or to the whole heterodimer. Thus, an aptamer-antibody correlation study was performed using $CD49d^{+}CD29^{+}$ H9 cells, $CD49d^{+}CD29^{+}$ Jurkat cells, and $CD49d^{-}$ $CD29^{+}$ K562 cells (Figure 2).

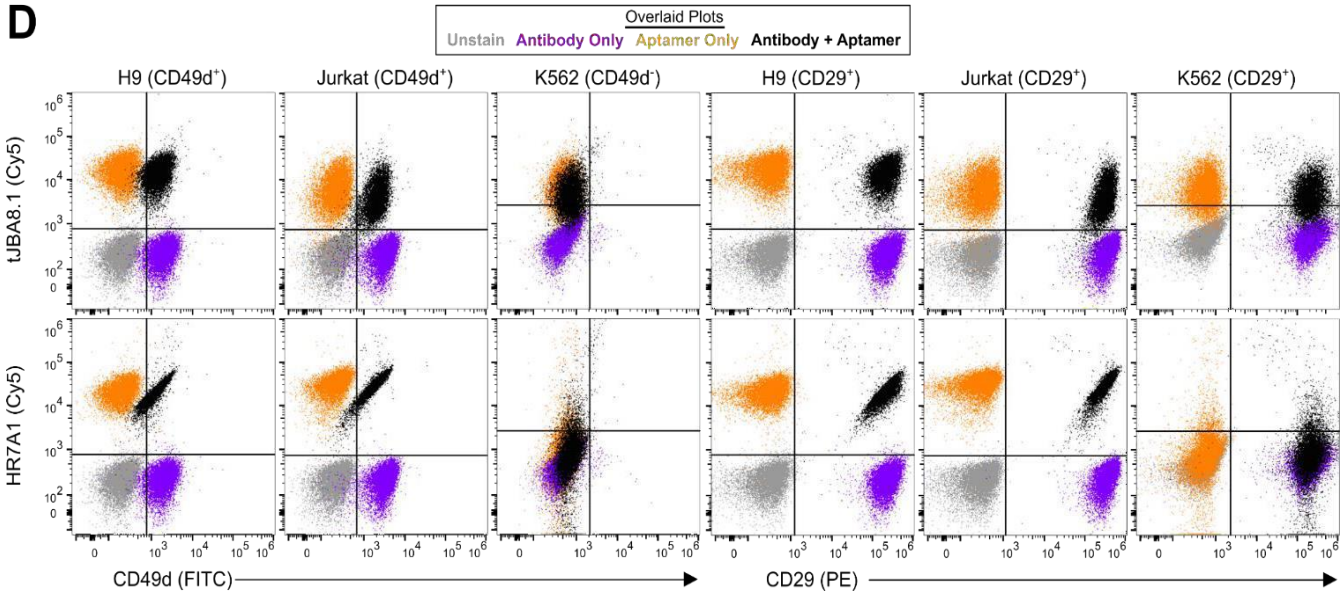

Figure 2. Aptamer-antibody correlation study in $CD49d^{+}CD29^{+}$ H9, $CD49d^{+}CD29^{+}$ Jurkat, and $CD49d^{-}CD29^{+}$ K562 cells.

The data showed a clear correlation between CD49d expression and HR7A1 binding in both H9 and Jurkat cells compared to the control. Correlation was also observed between CD29 expression and HR7A1 in both H9 and Jurkat cells. The aptamer showed a complete lack of binding to K562 cells, indicating that the presence of just the CD29 subunit is not sufficient for HR7A1 binding. Although the data shown in Figure 2 might indicate the propensity for HR7A1 to bind the integrin heterodimer, it is important to note that CD49d expression itself might correlate with CD29 expression. That is, CD49d may be stoichiometrically expressed with CD29 at a 1:1 ratio and is only present as heterodimer. This would result in aptamer binding indirectly correlating with CD29 via binding of CD49d. A subsequent antibody-antibody correlation study showed roughly 1:1 expression of CD29 and CD49d, suggesting that the HR7A1-CD29 binding correlation observed previously could be indirectly caused by HR7A1 binding to CD49d (Figure 3). Due to this relationship, further studies were necessary to fully illuminate the receptor target of HR7A1.

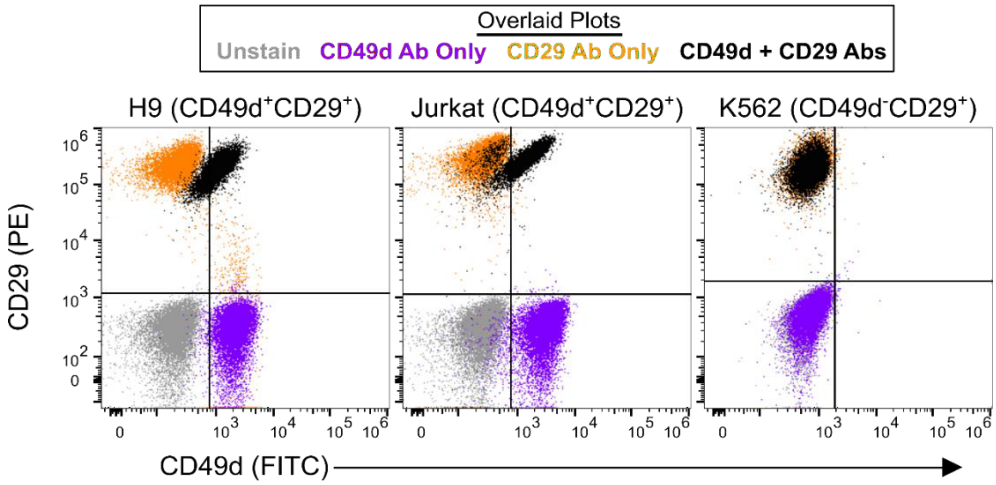

Figure 3. CD49d-CD29 correlation study H9, Jurkat, and K562 cells.

To definitively confirm the binding target of HR7A1, a CD29 knockdown study was performed using siRNA nucleofection. Binding was evaluated after 42 hours post-nucleofection across three technical replicates of Jurkat cells. The data revealed that HR7A1 closely matched

CD29 antibody binding (Figure 4). Although CD49d expression was also reduced in the process, the reduction in aptamer binding aligned considerably more with the reduction in CD29 expression.

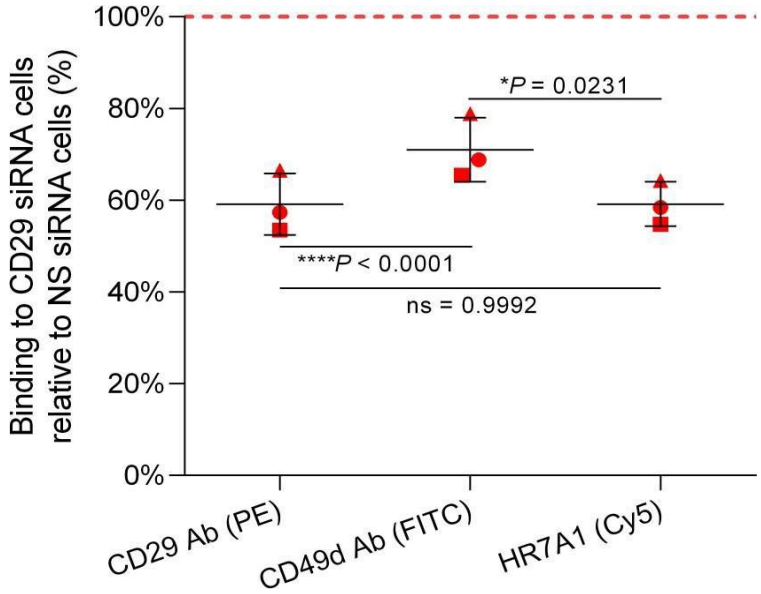

Figure 4. CD29 siRNA knockdown and subsequent HR7A1 binding on Jurkat cells in three technical replicates. Paired one-way ANOVA with Tukey's multiple comparisons to test for significance.

A paired one-way ANOVA with Tukey's multiple comparisons test was performed to determine the statistical significance of the data. The significance test revealed that both HR7A1 binding and CD29 expression were significantly different from CD49d expression across all three replicates. Furthermore, no significant was difference observed between the HR7A1 binding and CD29 expression within each replicate. This data strongly suggested that HR7A1 targeted the α4β1 heterodimer and not just the α4 integrin. However, for further validation that the entire α4β1 heterodimer was necessary for aptamer binding, the association and dissociation kinetics of integrin-aptamer binding were measured using bio-layer interferometry. Integrins α4β1 and α4β7 were screened against HR7A1 and control aptamers immobilized onto BLI sensors. The data revealed that HR7A1 bound α4β1 with single-digit nanomolar affinity, with more than 10-fold higher affinity for α4β1 than α4β7. This data, in conjunction with prior studies, allowed us to

definitively conclude that the HR7A1 aptamer targeted the whole α4β1 heterodimer and neither subunit alone.

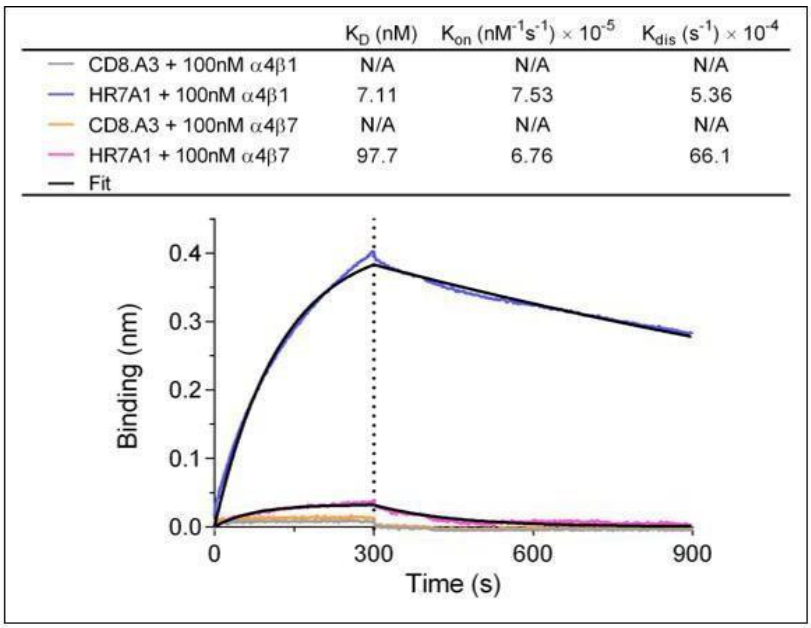

Figure 5. Association and dissociation kinetics of α4β1 and α4β7 integrins binding to immobilized HR7A1 and control aptamer

It is important to mention that a CD49d-specific aptamer, dubbed Sgc4f, has already been discovered and characterized by the Tan group at the University of Florida [17]. As such, we sought to compare the binding properties of Sgc4f to HR7A1 and its truncated variants by producing binding curves for each aptamer against K562, H9, and Jurkat cells (Figure 6). HR7A1 Trunc1 1 ($K_D \simeq$ 0.9-1.5nM) and Trunc2 ($K_D \simeq$ 1-1.7nM) both demonstrated roughly 2-fold improved apparent affinity over full-length HR7A1 ($K_D \simeq$ 2-3nM). Sgc4f ($K_D \simeq$ 2-4.7nM) displayed either comparable or lower affinity than full-length HR7A1, depending on the cell line, and considerably lower affinity than both truncations of HR7A1.

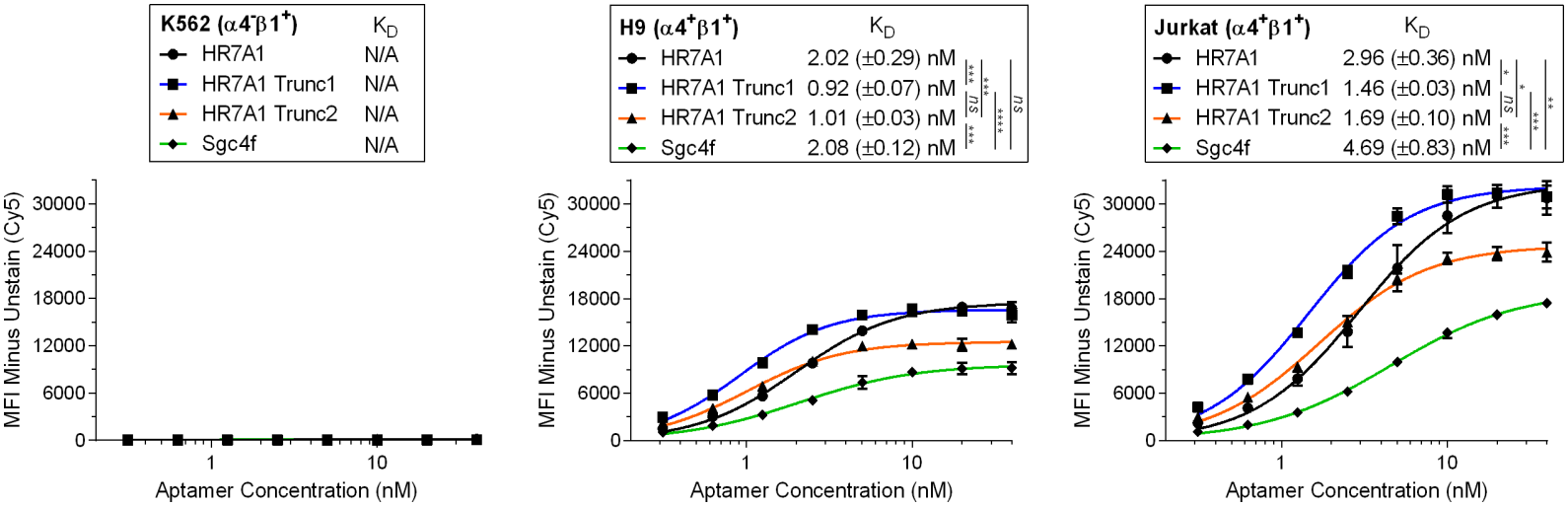

Figure 6. Binding curves for HR7A1, Trunc1, Trunc2, and Sgc4f on K562 ($CD29^+CD49d^-$), H9 ($CD29^+CD49d^+$), and Jurkat cells ($CD29^+CD49d^+$)

A binding study was performed using PBMCs isolated from three distinct blood donors to evaluate the cancer selectivity of the aptamer (Figure 7). The results showed significantly higher binding to H9 T-lymphoma and Jurkat T-leukemia cell lines than healthy cells. Although the aptamer did not demonstrate full cancer specificity, the cancer selectivity of the aptamer was established based on the minimal binding observed to healthy PBMCs.

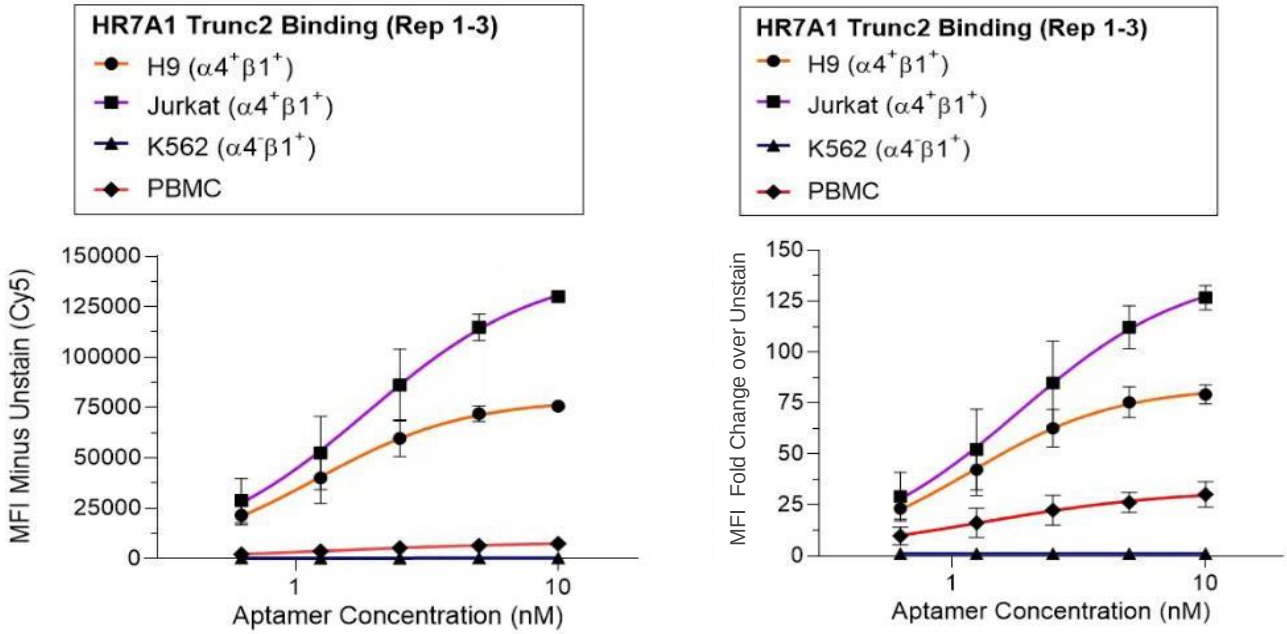

Figure 7. HR7A1 Trunc2 binding against three biological replaces of H9, Jurkat, K562, and PBMCs. Data for both raw binding MFI (left) and MFI fold change (right) are shown.

II. Serum Stability Analysis

Various modifications for the aptamer were then proposed to improve its serum half-life, including the design of dimerized aptamers, 3' inverted dT caps, and bioconjugation to larger molecules. Analysis of existing literature revealed 2' O-methylation as a potent mitigator of nuclease degradation, with multiple aptamer research groups highlighting improvements in aptamer stability post-modification. Structural analysis of the HR7A1 Trunc2 aptamer on the NUPACK tool and evaluation of highly mutated bases among top ranking aptamers from the SELEX informed us of the optimal sites for modification (Figure 8).

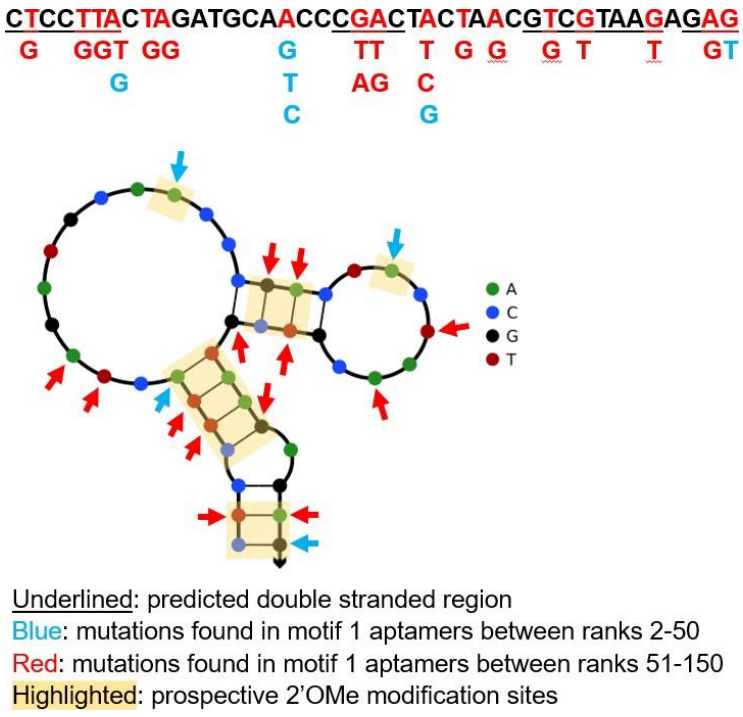

Figure 8. NUPACK predicted structure of HR7A1 Trunc2 with prospective modification sites highlighted. Common mutations in rank 2-150 aptamers marked in red and blue.

The highlighted locations were most amenable to modification as they exhibited the highest variation in nucleobase identity across the top aptamers from the SELEX process. Of the total potential modification options, only four bases—two bases at the 3' end and two bases at the 5' end of the single-stranded DNA sequence—were chosen to be modified. These bases are highlighted in Figure 9.

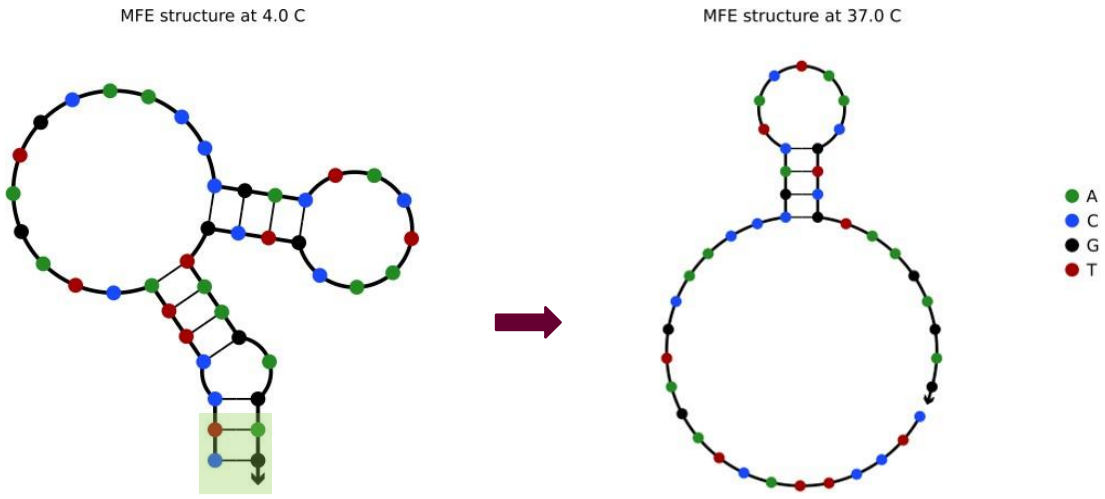

Figure 9. NUPACK simulated structure of HR7A1 Trunc2 at 4C and 37C (0.137M Na+, 0.0055M Mg++) Bases chosen for 2'-O-Methyl modification highlighted in green.

The binding characteristics of the modified HR7A1 Trunc2 2'OMe aptamer were subsequently evaluated, and it was found that the modifications did not negatively impact binding compared to unmodified HR7A1 Trunc2. Serum stability studies revealed no improvement in serum stability to unmodified aptamers, with no significant differences in serum half-life observed between the groups across two replicates (Figure 10). Nonetheless, the unmodified aptamer was able to maintain at least half-maximal binding serum for multiple hours; this would enable the aptamer to effectively circulate and function in vivo before undergoing nuclease degradation.

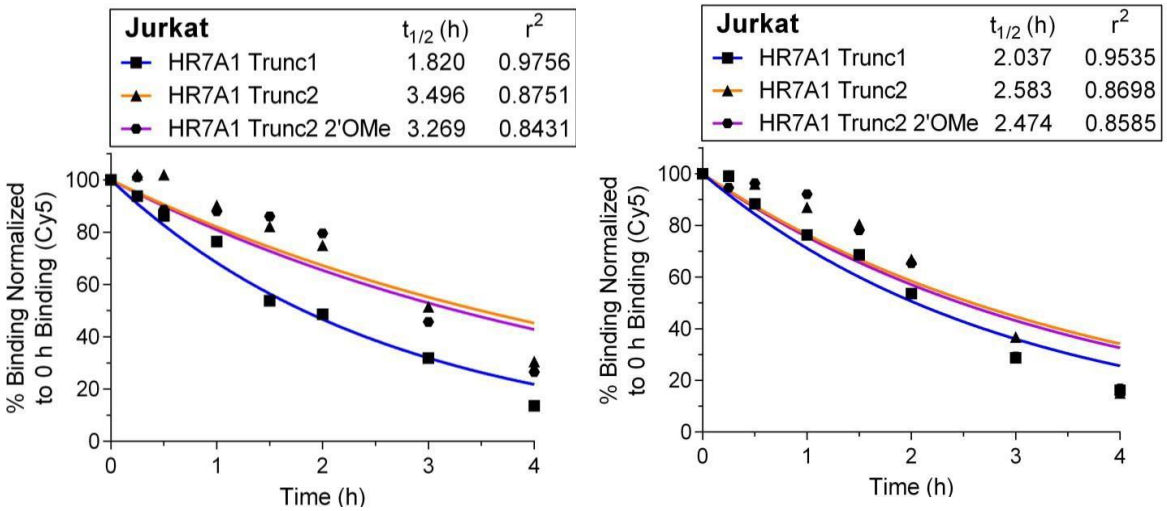

Figure 10. Binding capabilities of HR7A1 Trunc1, Trunc2, and Trunc2 2'OMe after incubation in normal mouse serum for varying timepoints. Normalized to binding after 0h incubation.

III. Thermal Stability Improvement

Conformational stability is another characteristic of aptamers that we wished to improve. Unlike proteins, aptamers are not irreversibly denatured at high temperatures and will snap back to their original conformation upon cooling. However, aptamers may assume different 3D conformations at higher temperatures, which may result in reduced binding affinity. As shown in Figure 9, the unmodified HR7A1 Trunc2 aptamer is simulated to adopt a drastically different conformation at 37C compared to 4C, which may result in loss of binding. Thus, the binding capabilities of HR7A1 Trunc2 and Trunc2 2'OMe were tested at 37C to ensure that the aptamers retain binding at in vivo temperatures. We hypothesized that the theoretical increase in melting temperature from the 2'OMe RNA pairs would increase the thermal stability of the aptamer's 4C structure, thereby retaining more binding when used at 37C. Indeed, binding only decreased by 52-71% at the 37C conditions for the 2'OMe modified aptamer, an estimated 15-20% improvement over the unmodified aptamer (Figure 11).

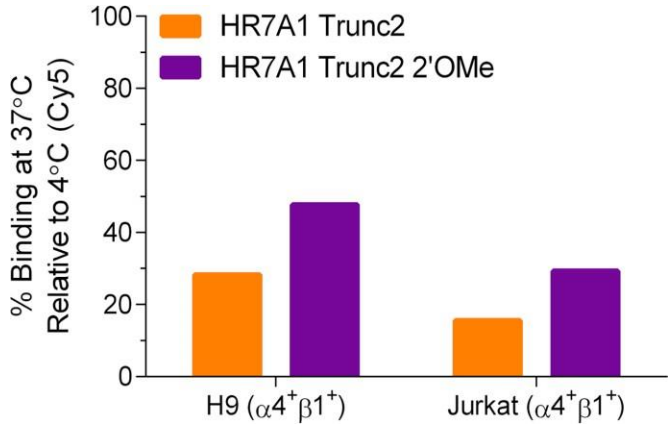

Figure 11. Normalized HR7A1 Trunc2 and Trunc2 2'OMe binding at 37C relative to 4C.

Nevertheless, there was still a large discrepancy between 37C and 4C binding, and the minor improvement in thermal stability did not justify the high cost of the 2'OMe modification. A primary goal of our thermal stability optimization process was for our final aptamer to retain at

least 50% binding at 37C compared to 4C. To this end, we pursued further modification of the HR7A1 Trunc2 aptamer to increase its thermal stability via base-pair substitution, base-pair addition, as well as various combinations of the two approaches. Additionally, a nucleotide in the internal duplex of the aptamer was modified to be a locked nucleic acid (LNA). LNA-DNA heteroduplexes have been shown to significantly increase thermal stability; furthermore, LNA pyrimidines contribute more to stability than LNA purines [18]. Thus, a thymine nucleobase was chosen for modification. The first three modified sequences can be found in Table 1, with HR7A1 Trunc2 listed as a point of reference.

Name	Sequence
HR7A1 Trunc2	CTCCTTACTAGATGCAACCCGACTACTAACGTCGTAAGAGAG
Trunc2, Stem Extension, One Pair Substitution (SubExt)	CGCGCCTTACTAGATGCAACCCGACTACTAACGTCGTAAGAGCGCG
Trunc2, Two Pair Substitutions (Sub2)	CGCCGTACTAGATGCAACCCGACTACTAACGTCGTACGAGCG
Trunc2, LNA Duplex (LNA)	CTCCTTACTAGATGCAACCCGACTACTAACG+TCGTAAGAGAG

Table 1. Initial aptamer modifications theorized to improve thermal stability of HR7A1 Trunc2. Bases highlighted in blue are substitutions (A/T to G/C), while bases in green are additions.

The binding capabilities of the modified aptamers were first tested to ensure the modifications did not negatively affect receptor specificity and affinity (Figure 12). Both the Sub2 and SubExt modifications retained binding affinity, with the K_D remaining at ~1nM. In contrast, the LNA modification was much less tolerated, with complete loss of binding. Although LNA modifications have been well-characterized as having anti-degradation properties, the “locked” nature of the nucleotide may have prevented folding of the aptamer into the correct 3D conformation necessary for binding.

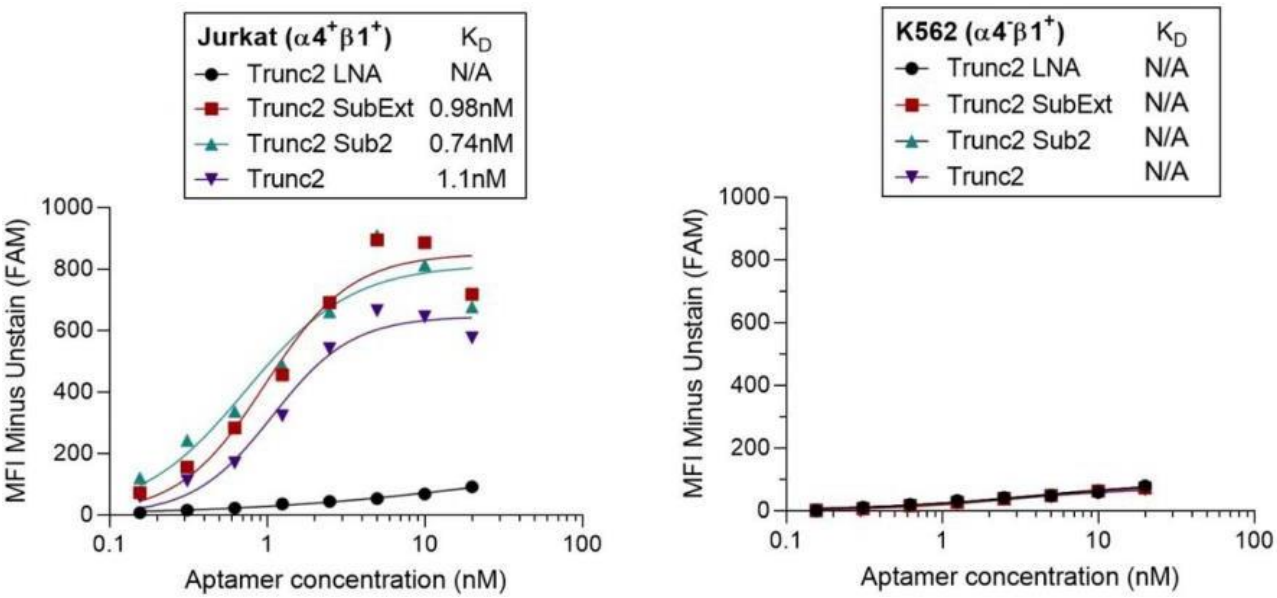

Figure 12. Binding curve of HR7A1 Trunc2, Trunc2 SubExt, Trunc2 Sub2, and Trunc2 LNA

The conformational stability of the aforementioned aptamers at 37C were then evaluated. Two changes were made to the thermal stability protocol to test the stability of the aptamers at 37C more rigorously, as outlined in Table 2. This modified protocol was used in all subsequent experiments. This was done to simulate the in vivo environment more accurately, to help ensure that the in vitro optimization translated into improved thermal stability in mouse models.

Modification	Initial protocol	Modified protocol
Pre-equilibration of cells at 37C	N/A	10 minutes
Pre-equilibration of aptamer at 37C	N/A	30 minutes
Aptamer-cell incubation at 37C	30 minutes	30 minutes

Table 2. List of modifications to improve thermal stability protocol

The results of thermal stability study are presented in Figure 13, with each aptamer's MFI normalized to their respective binding MFI at 4C. The stem stabilizing modifications both made a

positive impact on conformational stability at 37C, with a roughly 10% improvement in 37C binding MFI. Although promising, higher thermal stability was necessary to maintain efficacy in vivo.

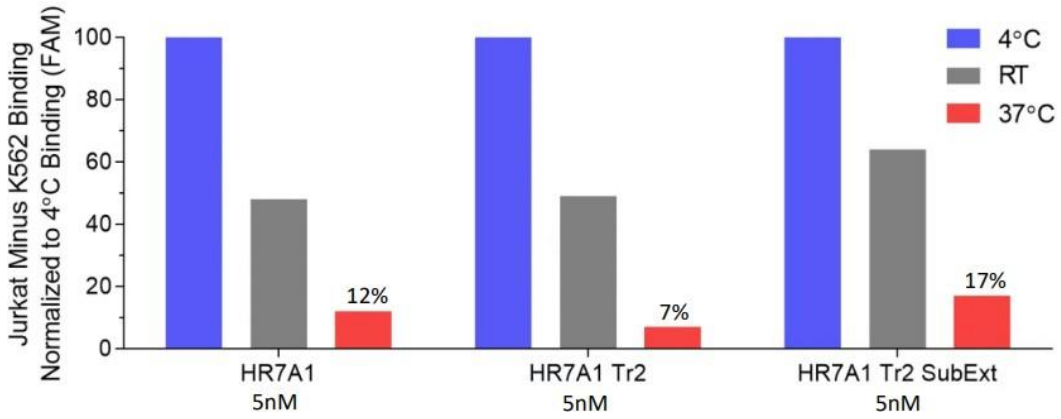

Figure 13. Binding MFI of full-length HR7A1, HR7A1 Trunc2, and HR7A1 SubExt at 4C, 20C, and 37C. Normalized to 4C binding.

Since none of the modifications reached the goal of >50% retention of 4C binding at 37C, further modifications were explored. First, the previous stem substitutions (Sub2) and the extensions (SubExt) were combined to produce HR7A1 Trunc2 Sub2Ex2. Using Sub2Ex2 as a base, we further stabilized the internal duplex by swapping the only AT pair in the duplex with GC to create HR7A1 Trunc2 GCDup (Figure 14).

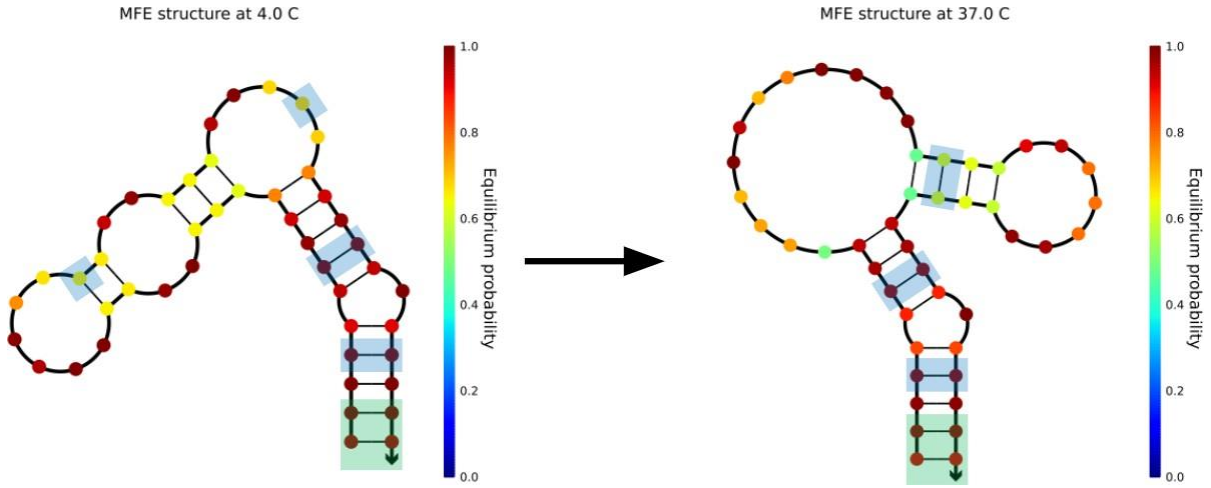

Figure 14. NUPACK predicted structure of HR7A1 Trunc2 GCDup. Bases highlighted in blue are substitutions (A/T to G/C), while bases in green are GC additions.

Although the predicted structure of the Trunc2 GCDup sequence at 4C was different from the unmodified HR7A1 Trunc2 structure, the aptamer had the correct predicted structure at 37C. Lastly, we substituted a base outside of the internal duplex that indirectly stabilizes the internal duplex. The predicted secondary structure of HR7A1 Trunc2 Sub2Ex2 at 37C revealed that the only nucleobases with low equilibrium probability were those in the internal duplex and a single-stranded C nucleobase in position 10 from the 5' end (Figure 15).

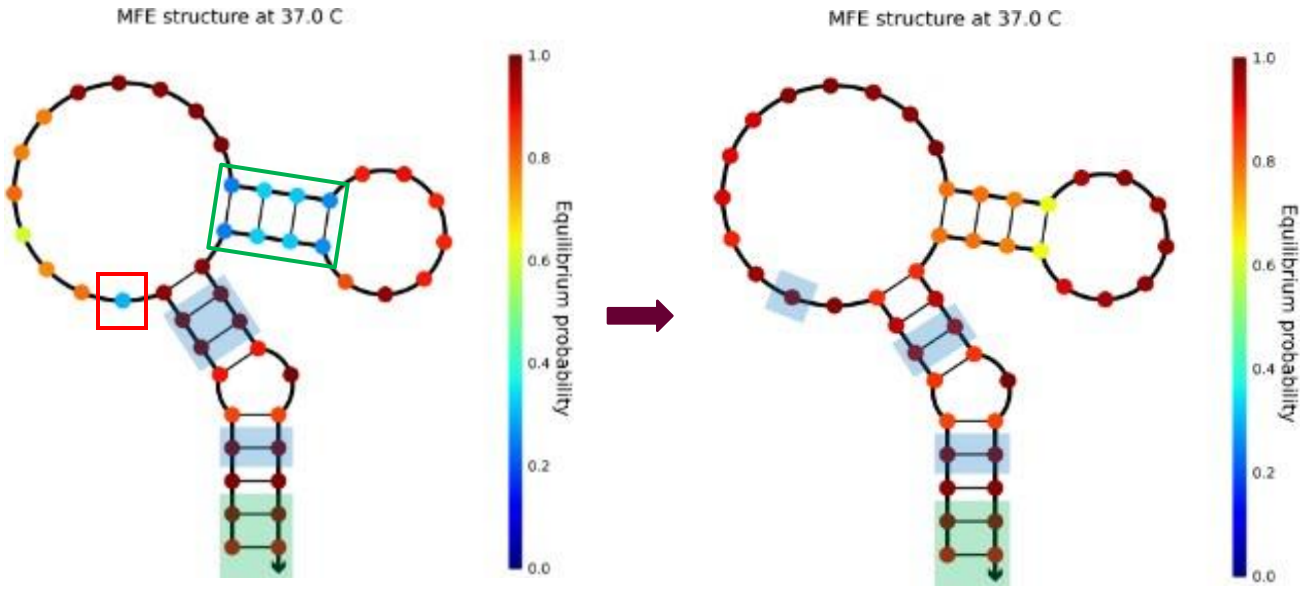

Figure 15. NUPACK predicted structures of HR7A1 Trunc2 Sub2Ex2 (left) and A10 (right). Single-stranded C nucleobase marked in red. Internal duplex requiring stabilization marked in green.

Assuming that the NUPACK predicted structures were accurate, this suggested that the single-stranded C nucleobase was destabilizing the internal duplex by attempting to base pair with the most proximal G nucleobase in the duplex. To prevent this, we substituted this C nucleobase with either A or T nucleobases, significantly stabilizing the internal duplex. These two sequences were named HR7A1 Trunc2 Sub2Ex2 A10 and T10 and have been listed in the table below alongside the sequences for Sub2Ex2 and Sub2Ex2 GCDup.

Name	Sequence
HR7A1 Trunc2	CTCCTTACTAGATGCAACCCGACTACTAACGTCGTAAGAGAG
Trunc2, Stem Extension, Two Pair Substitution (Sub2Ex2)	CGCGCCGTACTAGATGCAACCCGACTACTAACGTCGTACGAGCGCG
Trunc2 Sub2Ex2, with GC duplex (GCDup)	CGCGCCGTACTAGATGCAACCCGGCTACTAACGCCGTACGAGCGCG
Trunc2 Sub2Ex2, adenine substitution (A10)	CGCGCCGTAATAGATGCAACCCGACTACTAACGTCGTACGAGCGCG
Trunc2 Sub2Ex2, thymine substitution (T10)	CGCGCCGTATTAGATGCAACCCGACTACTAACGTCGTACGAGCGCG

Table 3. Second set of aptamer modifications to improve thermal stability of HR7A1 Trunc2. Bases highlighted in blue are substitutions (A/T to G/C), while bases in green are additions.

A binding study was then performed with Trunc2 GCDup, Trunc2 A10, and Trunc2 T10, which revealed that the A10 aptamer did not saturate even at 50nM concentrations, indicating that it binds with significantly reduced affinity compared to unmodified Trunc2. On the other hand, both the GCDup and T10 aptamers demonstrated moderate binding ($K_D \simeq$ 4.5nM), with only 4-5X lower affinity than unmodified HR7A1 Trunc2 ($K_D \simeq$ 1nM). Thus, we proceeded with thermal stability evaluations of the three aptamers shown in Figure 16.

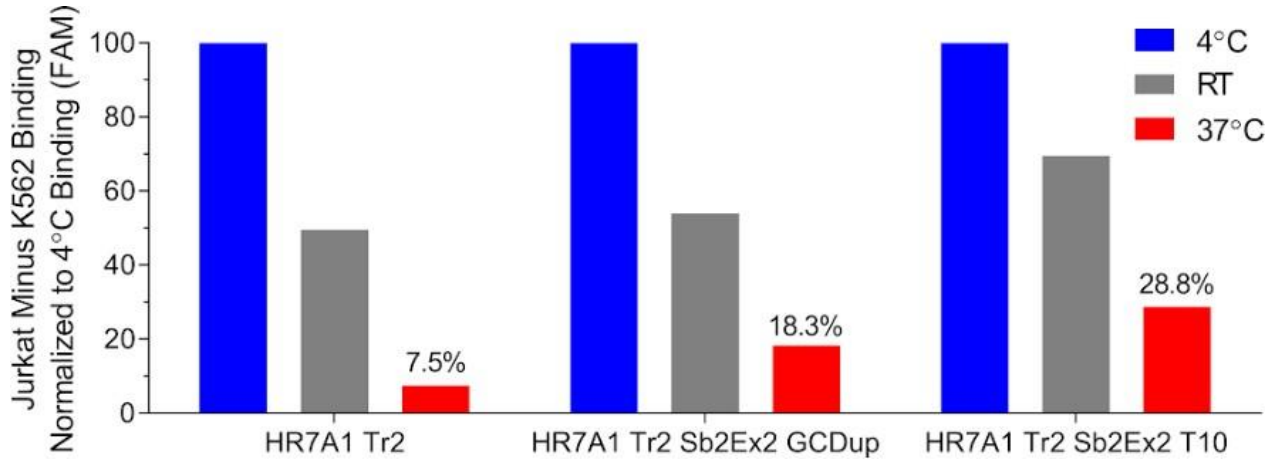

Figure 16. Binding characteristics of HR7A1 Trunc2, Sub2Ex2 GCDup, and Sub2Ex2 T10 at 4C, 20C, and 37C. Normalized to 4C binding.

Both GCDup and T10 aptamers demonstrated a marked improvement in binding at 37C, retaining 18.3% and 28.8% of their respective 4C binding MFI at 37C. However, the modifications still had not reached the desired >50% retention of binding at 37C. One new modification was to create a CGDup aptamer, reversing the positions of the G and C nucleobases from the GCDup aptamer. Although this change was predicted to slightly destabilize the aptamer stem, we were confident that the Sub2Ex2 modifications had already sufficiently stabilized the stem (Figure 17).

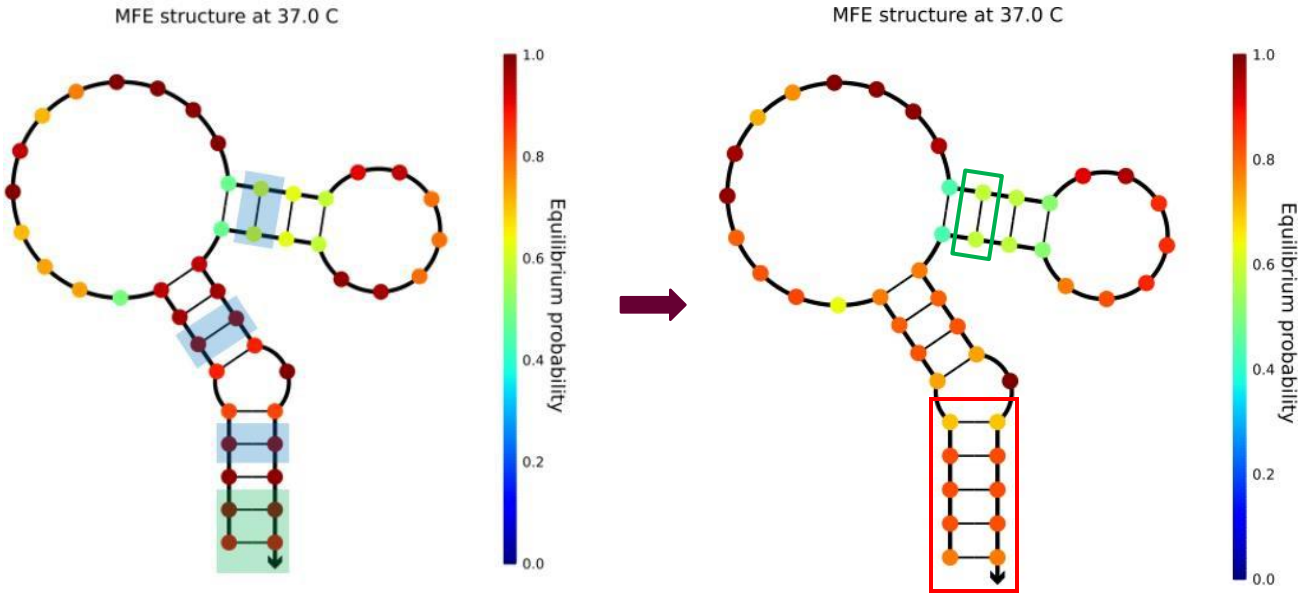

Figure 17. NUPACK predicted structures of HR7A1 Trunc2 Sub2Ex2 GCDup (left) and CGDup (right). Slightly de-stabilized stem in CGDup marked in red. CGDup location marked in green.

Another route to stabilize the internal duplex was to keep the original AT base pairing, but swap them for 2'OMe AU groups, making an mAUDup aptamer. Theoretically, the 2'OMe bases should have a higher melting temperature when paired together when paired as an RNA-DNA heteroduplex. One additional pair substitution was possible to further stabilize the aptamer stem was to add another AT>GC substitution, making the Sub3Ex2 aptamer. The sequences of the aforementioned aptamers are listed below in Table 4.

Name	Sequence
Trunc2, Stem Extension, Two Pair Substitution (Sub2Ex2)	CGCGCCGTACTAGATGCAACCCGACTACTAACGTCGTACGAGCGCG
Trunc2 Sub2Ex2, with CG duplex (CGDup)	CGCGCCGTACTAGATGCAACCCGCCTACTAACGGCGTACGAGCGCG
Trunc2 Sub2Ex2, mAUDup (mAUDup)	CGCGCCGTACTAGATGCAACCCGmACTACTAACGmUCGTACGAGCGCG
Trunc2, Stem Extension, Three Pair Substitution (Sub3Ex2)	CGCGCCGGACTAGATGCAACCCGACTACTAACGTCGTCCGAGCGCG

Table 4. Third set of aptamer modifications to improve thermal stability of HR7A1 Trunc2. Bases highlighted in blue are substitutions (A/T to G/C), while bases in green are additions.

CGDup ($K_D \simeq 2.3$nM) demonstrated comparable affinity to the original Tr2 aptamer ($K_D \simeq 3.1$nM), whereas Sub3Ex2 had slightly lower affinity ($K_D \simeq 6.4$nM). Sub2Ex2 mAUDup did not display binding to Jurkats above the α4- K562 controls; this suggested that "unnatural" bases were unsuitable for substitution into the duplex, as a similar result was observed with the LNA modification.

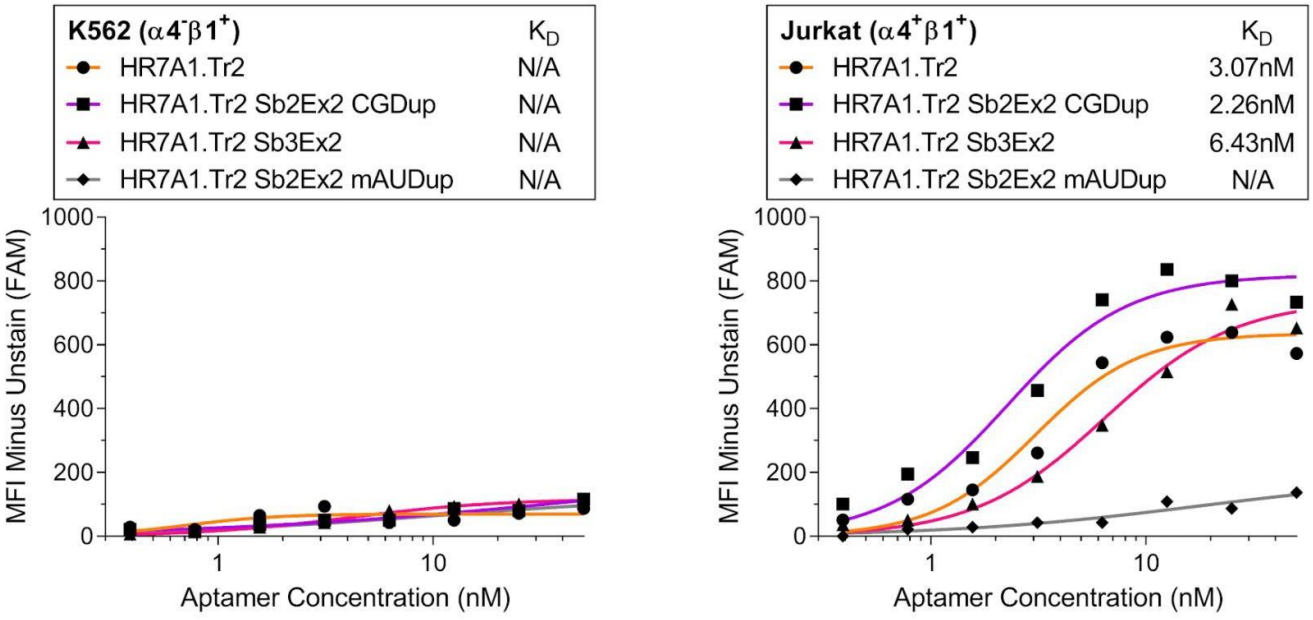

Figure 18. Third set of aptamer modifications to improve thermal stability of HR7A1 Trunc2. Bases highlighted in blue are substitutions (A/T to G/C), while bases in green are additions.

We then tested the thermal stability of Sub2Ex2 CGDup and Sub3Ex2 and observed minimal improvements in 37C binding (Figure 19). These thermal stability improvements were more modest than the previous round of modifications could have potentially been due to the CGDup modification destabilizing the stem relative to GCDup, whereas Sb3Ex2 only further stabilized an already stable stem, relative to Sub2Ex2.

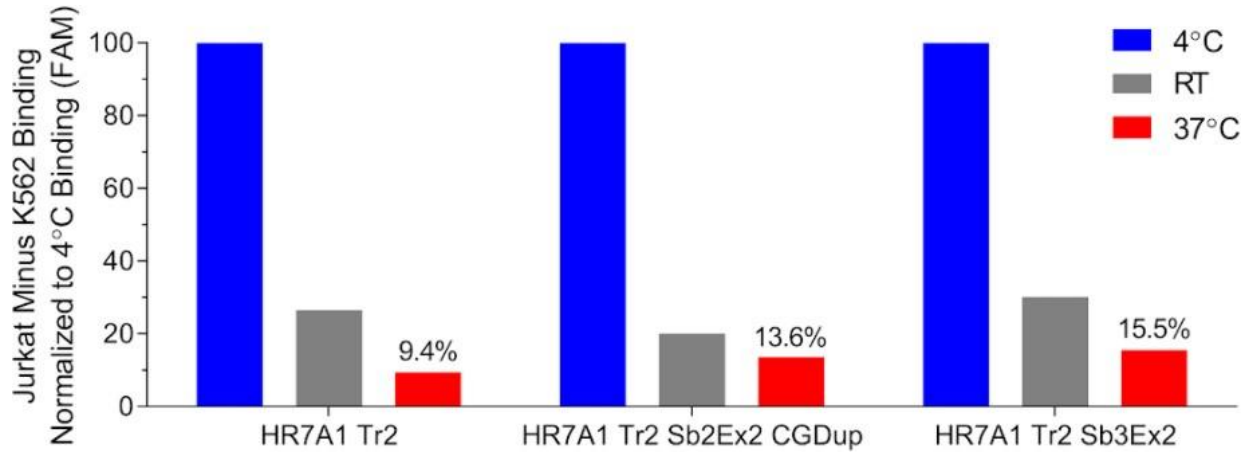

Figure 19. Binding characteristics of HR7A1 Trunc2, Sub2Ex2 CGDup, and Sub3Ex2 at 4C, 20C, and 37C. Normalized to 4C binding.

Summarizing the data thus far: Sub2Ex2 and Sub3Ex2 stem modifications did not substantially improve thermal stability on their own and differentially impacted affinity, with Sub2Ex2 binding with higher affinity than Sub3Ex2 (Figures 16, 19). Additionally, the T10 modification in the single-stranded hairpin region indirectly stabilized the internal duplex with only a 2.5-fold reduction in affinity. Lastly, the GCDup and CGDup modifications in the internal duplex differentially impacted affinity, with CGDup binding more strongly than GCDup, and thermal stability, with GCDup demonstrating more conformational stability than CGDup at 37C (Figures 16, 19). This resulted in four possible aptamer sequences to combine these modifications as outlined in Table 5.

Name	Sequence
Trunc2 Sub2Ex2, T10 GCDup	CGCGCCGTATTAGATGCAACCCGGCTACTAACGCCGTACGAGCGCG
Trunc2 Sub3Ex2, T10, GCDup	CGCGCCGGATTAGATGCAACCCGGCTACTAACGCCGTCCGAGCGCG
Trunc2 Sub2Ex2, T10 GCDup	CGCGCCGTATTAGATGCAACCCGCCTACTAACGGCGTACGAGCGCG
Trunc2 Sub3Ex2, T10, GCDup	CGCGCCGGATTAGATGCAACCCGCCTACTAACGGCGTCCGAGCGCG

Table 5. Fourth round of aptamer modifications to improve thermal stability of HR7A1 Trunc2. Sequence not pursued shown in red, due to the minimal benefit of Sub3Ex2 combining with T10.

Analysis on NUPACK revealed that the addition of Sub3Ex2 over Sub2Ex2 to T10 and GCDup made minimal difference and actually slightly decreased equilibrium probabilities. In contrast, Sub3Ex2 was simulated to reverse the stem destabilizations that was introduced when CGDup is paired with Sub2Ex2. However, with the addition of T10, the structure was able to maintain stability. Informed by the predictive modeling software, we evaluated the following aptamers: Trunc2 Sub2Ex2 T10 GCDup, Trunc2 Sub2Ex2, T10 CGDup, and Trunc2 Sub3Ex2 T10 CGDup. The binding curves for the aptamers can be found in Figure 20.

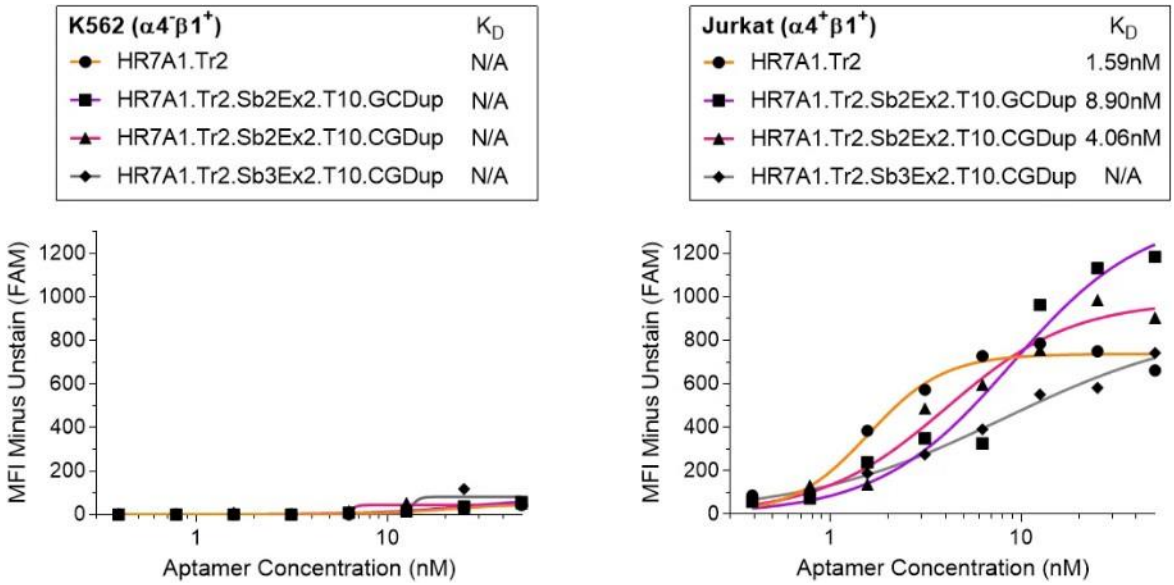

Figure 20. Binding curve for Trunc2 Sub2Ex2 T10 GCDup, Trunc2 Sub2Ex2, T10 CGDup, and Trunc2 Sub3Ex2, T10 CGDup.

Both Sub2Ex2 T10 GCDup ($K_D \simeq$ 8.9nM) and Sub2Ex2 T10 CGDup ($K_D \simeq$ 4.1nM) demonstrated lower affinity binding than unmodified HR7A1 Trunc2 ($K_D \simeq$ 1.6nM). Sub3Ex2 T10 CGDup binding did not saturate up to 40nM, indicating that it binds with drastically reduced affinity compared to unmodified Trunc2. Nevertheless, the three aptamers were evaluated for conformational stability at 37C (Figure 21).

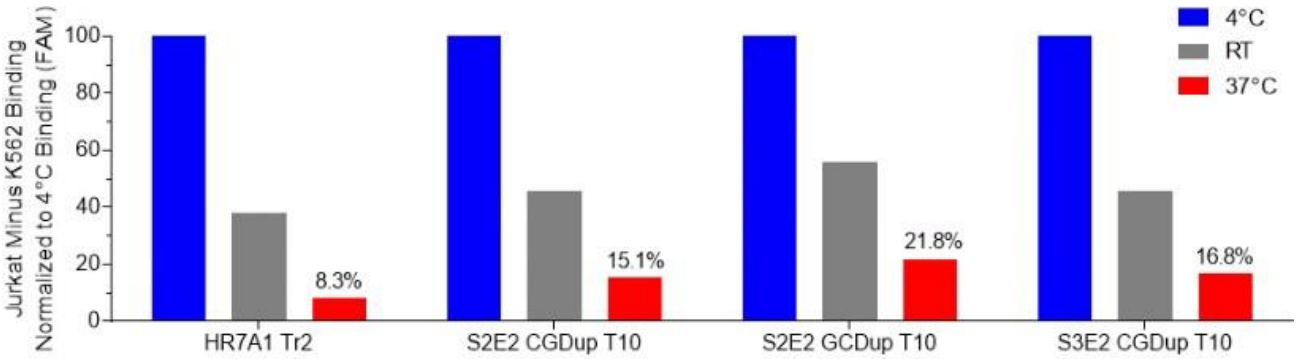

Figure 21. Binding characteristics of HR7A1 Trunc2, Sub2Ex2 T10 GCDup, Sub2Ex2 T10 CGDup, and Sub3Ex2 T10 CGDup at 4C, 20C, and 37C. Normalized to 4C binding.

The Sub2Ex2 GCDup 10 aptamer demonstrated the highest thermal stability of 21.8% binding at 37C relative to 4C. Both the Sub2Ex2 and Sub3Ex2 variants of CGDup T10 demonstrated ~16% binding retention. This exhausted all available options for aptamer mutations, as we had modified all of the amenable nucleobases highlighted in **(**Figure 8**).** A full binding curve of the top performing thermally stable aptamers (Sub2Ex2 T10, Sub2Ex2 T10 GCDup, and Sub2Ex2 T10 CGDup) at 37C was then created. The results demonstrated a rapid internalization of the aptamers at 37C. At 4C, aptamer binding saturates at higher concentrations as increasingly more of the available receptors on the cell surface become occupied. However, the aptamer-receptor complex is internalized at 37C, leading to the exponential binding curve seen in Figure 22.

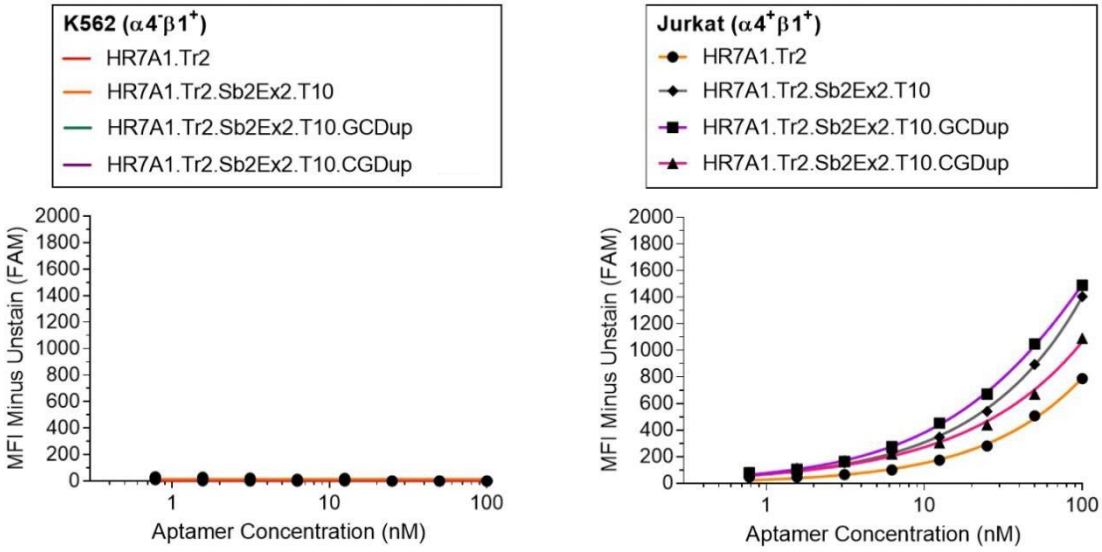

Figure 22. 37C binding curve of the most thermally stable aptamers on Jurkat and K562 cells.

The results from the studies conclusively determined that HR7A1 Trunc2 Sub2Ex2 T10 GCDup had the highest thermal conformational stability and was selected for further testing. The aptamer, renamed HR7A1 Trunc2 TS, was modified with a Cy5 fluorophore instead of the 6-FAM fluorophore that was present on the aptamers used for optimization. This allowed for higher sensitivity fluorescence readings for future studies. A binding curve for HR7A1 Trunc2 TS ($K_D \simeq$ 4.0nM) revealed ~4-5X lower binding than HR7A1 Trunc2 ($K_D \simeq 0.85$).

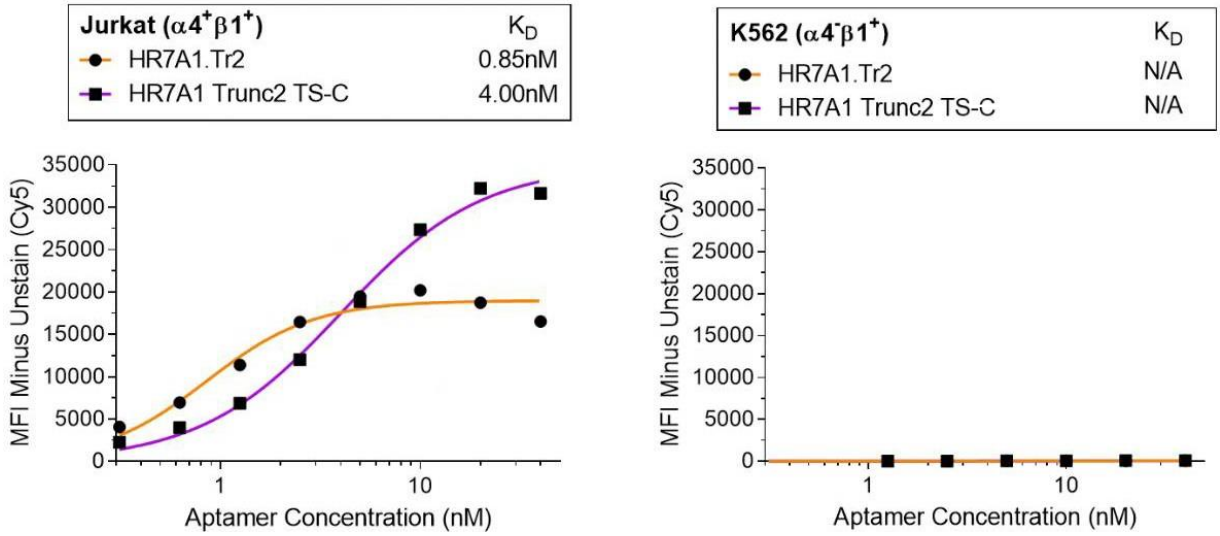

Figure 23. Binding curve of HR7A1 Trunc2 and HR7A1 Trunc2 TS against Jurkat and K562 cells

Thermal stability evaluation of the Trunc2 TS aptamer revealed ~2X higher binding at 37C than unmodified Trunc2, relative to their respective 4C binding MFIs. The 14.4% retention in binding MFI at 37C for HR7A1 Trunc2 signified a decrease from the aptamer it was based upon, the HR7A1 Trunc2 Sub2Ex2 T10 GCDup aptamer, with 21.8% retention. However, the 21.8% retention was calculated using the lower intensity, less sensitive fluorescent signals from the FAM fluorophore. The Cy5 fluorescence of the Trunc2 TS aptamer was determined to be a more reliable indicator of the true thermal stability of the aptamer at 37C.

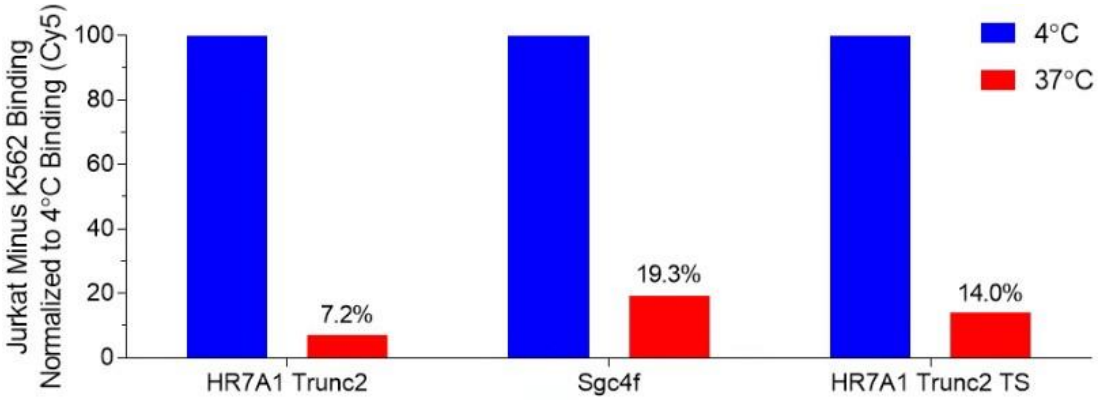

Figure 24. HR7A1 Trunc2, Sgc4f, and Trunc2 TS binding at 37C relative to 4C binding.

Although the goal of >50% retention in binding MFI at 37C relative to 4C was not achieved, we had exhausted our available nucleotide modification sites on the HR7A1 Trunc2 aptamer. Thus, we proceeded with the HR7A1 Trunc2 TS aptamer for further evaluation of the pharmacokinetic properties of the aptamer.

IV. Aptamer-Conjugate Constructs

Conjugation of the thiol-modified HR7A1 Trunc2 TS aptamer to DSPE-PEG(2000)-Maleimide, a lipidic albumin-targeting agent, was explored to improve circulation half-life via noncovalent association with albumin in vivo. Several rounds of testing were performed with a thiol-modified test aptamer via gel electrophoresis to determine optimal lipid-to-aptamer molar

ratios. The results, shown in Figure 25, revealed that a 100:1 molar ratio of lipid-to-aptamer produced the most efficient conjugation reaction. Increasing the lipid-to-aptamer molar ratio past 100:1 did not result in any significant decrease in unconjugated aptamer (Figure 25D). The aptamer-lipid conjugates also readily formed micelles, as shown by high molecular weight bands in Figure 25C.

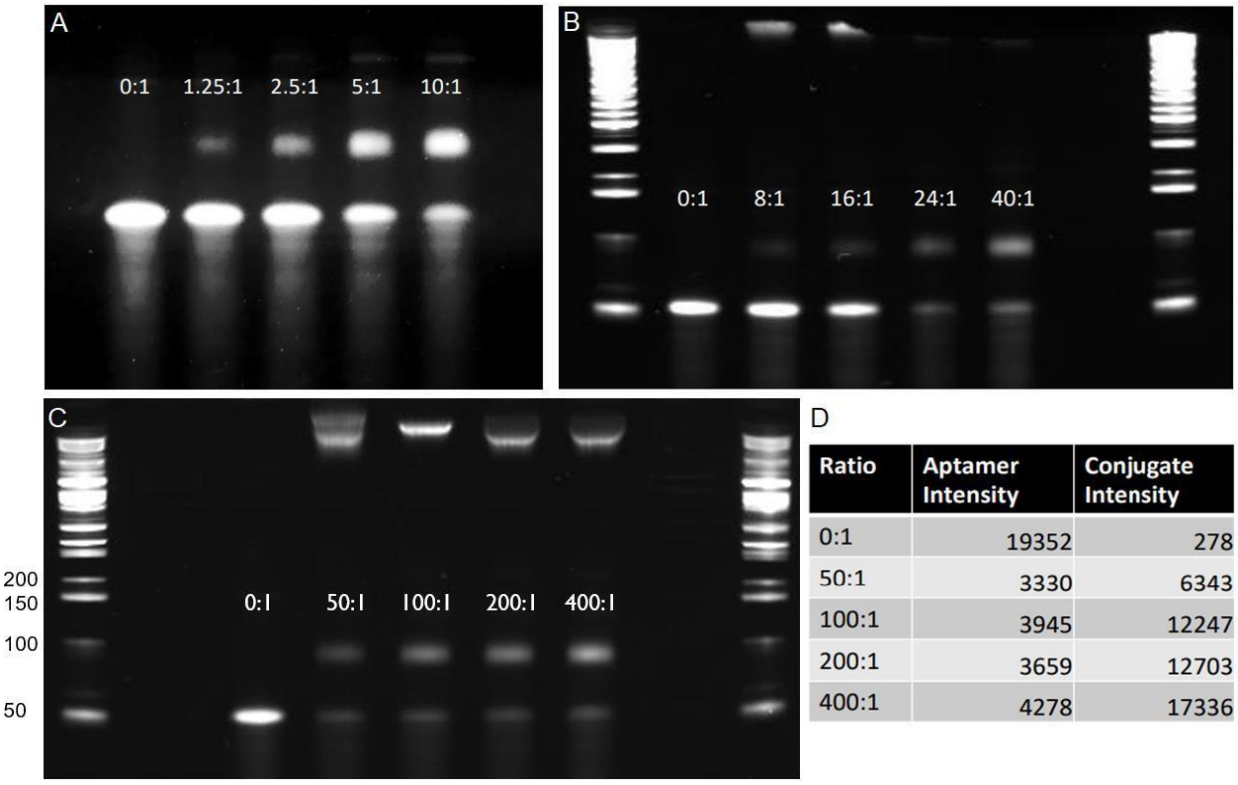

Ratio	Aptamer Intensity	Conjugate Intensity
0:1	19352	278
50:1	3330	6343
100:1	3945	12247
200:1	3659	12703
400:1	4278	17336

Figure 25. Gel shift assays to optimize molar ratios of DSPE-PEG(2000)-Maleimide to thiol-modified tJBA8.1 aptamer. (A) Lipid-to-aptamer molar ratios from 0:1 to 10:1. (B) Lipid-to-aptamer molar ratios from 8:1 to 40:1. (C) Lipid-to-aptamer molar ratios from 50:1 to 100:1. (D) ImageJ intensity analysis of unconjugated aptamer and conjugated aptamer bands from Fig. 4C.

DSPE-PEG(2000)-Maleimide was then conjugated with the thiol-modified HR7A1 Trunc2 TS aptamer at a 100:1 ratio. Gel electrophoresis was performed to validate the efficiency of the conjugation reaction (Figure 26). The results showed almost 100% conjugation efficiency at the tested molar ratio, a significant improvement from the reaction efficiency of test aptamer. This could have been a result of HPLC-purification of the Trunc2 TS aptamer post-synthesis, while the test aptamer was not synthesized with any purification steps.

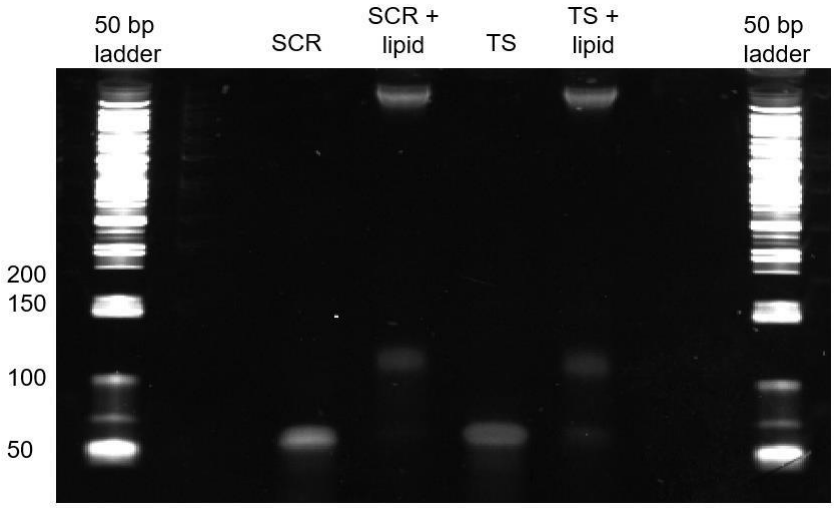

Figure 26. Gel-shift assay to validate reaction efficiency of the DSPE-PEG(2000)-Maleimide with the HR7A1 Trunc2 TS aptamer and the scrambled HR7A1 Trunc2 TS at a 100:1 molar ratio.

Gel electrophoresis was conducted to validate non-covalent association of the aptamer-lipid conjugate with albumin at 37C (Figure 27). Four conditions were tested: unconjugated SCRM-Trunc2-TS in DPBS, lipid-conjugated SCRM-Trunc2-TS in DPBS, unconjugated SCRM-Trunc2-TS with bovine serum albumin (BSA), and lipid-conjugated SCRM-Trunc2-TS with BSA.

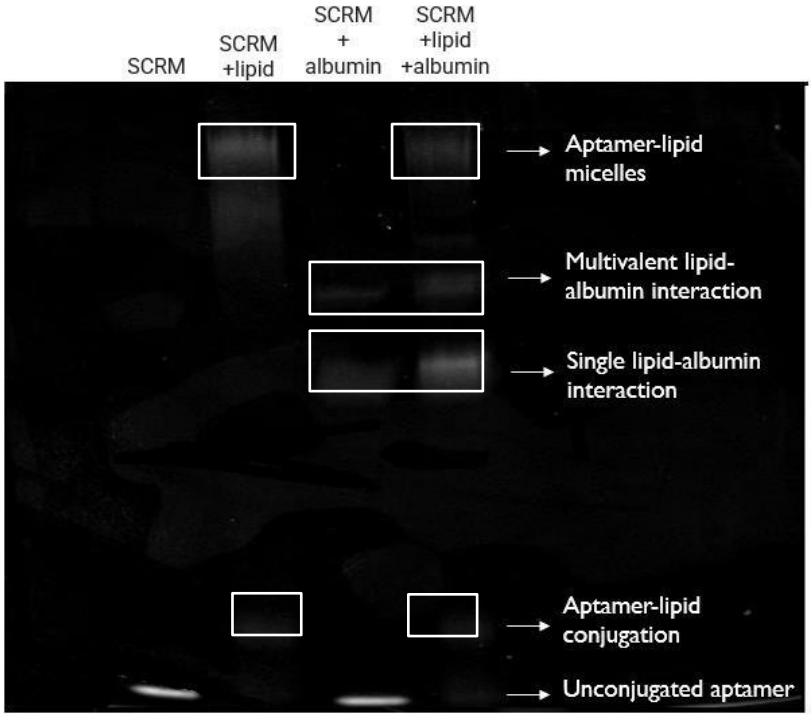

Figure 27. Gel-shift assay to validate non-covalent interactions between aptamer-lipid conjugate

and albumin protein

The results showed a tangible association between the lipid moiety of the aptamer conjugate and albumin protein. Although the unconjugated aptamer also demonstrated a minor association with albumin, the band intensity was noticeably higher in the presence of the lipid group. To characterize the in vivo pharmacokinetics of this aptamer, the circulation half-life was evaluated in immune-deficient mice. Despite expectations, the lipid-conjugated aptamer did not demonstrate higher circulation half-life compared to unmodified aptamer (Figure 28). No significant differences were observed between unmodified and lipid-conjugated aptamer fluorescence at 20- and 60-minutes post-injection. However, a significant increase in circulation of lipid-modified aptamer at 2min post-injection was observed. One theory to explain the discrepancy between the albumin-binding gel-shift assay and the in vivo circulation half-life relies on the in vivo characteristics of micelles. While the aptamer-lipid conjugate was incubated with albumin for 20 minutes before running micelles on the gel, no pre-incubation with albumin was included prior to aptamer injection into the mice. Since the aptamer-lipid conjugates exist primarily as micelles, it is possible that micelles did not break apart in circulation and expose the lipid moieties to albumin before renal filtration. The partial failure to robustly associate with albumin resulted in only a minimal increase in size between the unmodified and modified aptamers that was not enough to avoid the glomerular filtration size threshold.

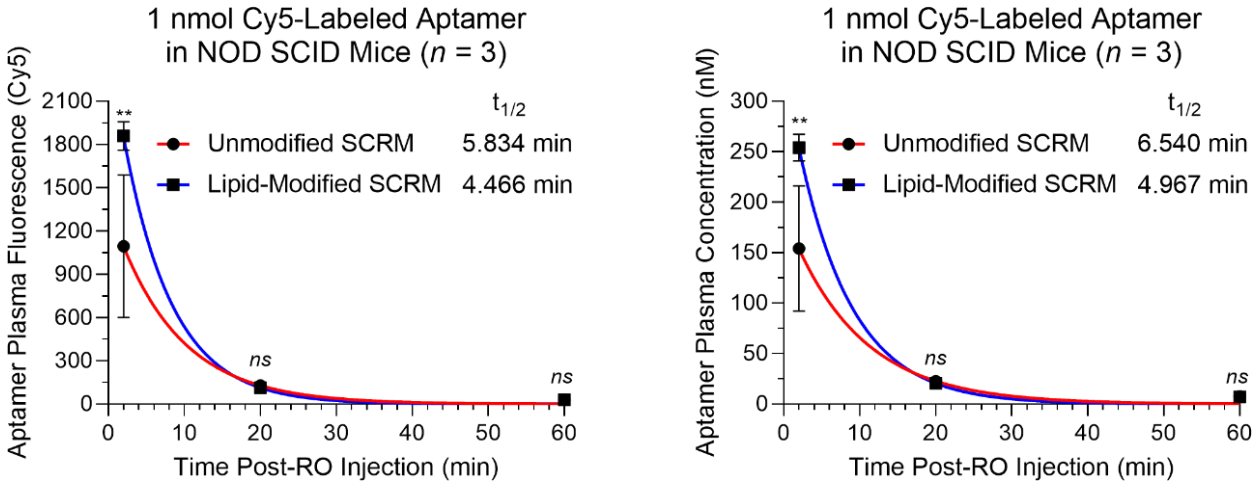

Figure 28. Circulation half-live of 1 nmol unmodified and modified aptamer in NOD SCID mice. Aptamer fluorescence measured using plasma from blood drawn at 2min, 20min, 60min

Polymer conjugation was then explored as an alternative method of improving the circulation half-life of the aptamer. Various polymers and conjugation strategies were tested, including thiol- and amine-modified aptamers with epoxide polymers; however, none yielded highly efficient aptamer-polymer conjugations. Copper-catalyzed cycloaddition of alkynes and azides, a procedure commonly referred to as "click reaction," is one promising alternative to traditional conjugation reactions [19]. However, the use of copper for oligonucleotide conjugation may result in metal-catalyzed strand degradation and difficulties in final purification [20]. Additionally, the Cu(I) catalyst is widely regarded as toxic and therefore incompatible with living cells due to its propensity for producing reactive oxygen species [21] Instead, copper-free click chemistries between cyclooctyne and azide groups have been utilized as non-toxic alternatives. To this end, the HR7A1 Trunc2 TS aptamer was modified with a dibenzo-cyclooctyne (DBCO) group and conjugated to a 25 kilodalton HPMA-AzP3MA polymer developed in our lab. Each polymer contained 30 azide groups available for conjugation with DBCO; thus, it was theoretically possible to attach up to 30 aptamers per polymer. However, given the large size of the aptamer (16.3kD) relative to the polymer backbone, steric clashes place a theoretical limit on the multivalency of the aptamer-polymer conjugate. The tested polymer-to-aptamer molar ratios can be found in the table below.

Condition	DBCO to Azide Ratio	Aptamer to Polymer Ratio
1	1:0	1:0
2	1:1	30:1
3	1:3	10:1
4	1:6	5:1
5	1:30	1:1
6	1:150	1:5
7	1:450	1:15
8	1:900	1:30

Table 6. List of DBCO-to-azide and aptamer-to-polymer molar ratios evaluated

A gel shift assay was conducted to visualize the conjugation efficiency of each reaction (Figure 29). At low polymer to aptamer ratios, when aptamer was in 10-fold and 30-fold excess of polymer, the reaction consisted of mostly high valency aptamer-polymer conjugates that did not migrate far into the gel. As more polymer was added, distinct bands began to appear further down the gel, representing lower valency conjugates. Reaction efficiency was calculated by measuring the intensity of the bands representing unconjugated aptamer. Using this metric, maximum reaction efficiency was observed to be at roughly a 5:1 aptamer-to-polymer ratio; this ratio was subsequently selected for further evaluation.

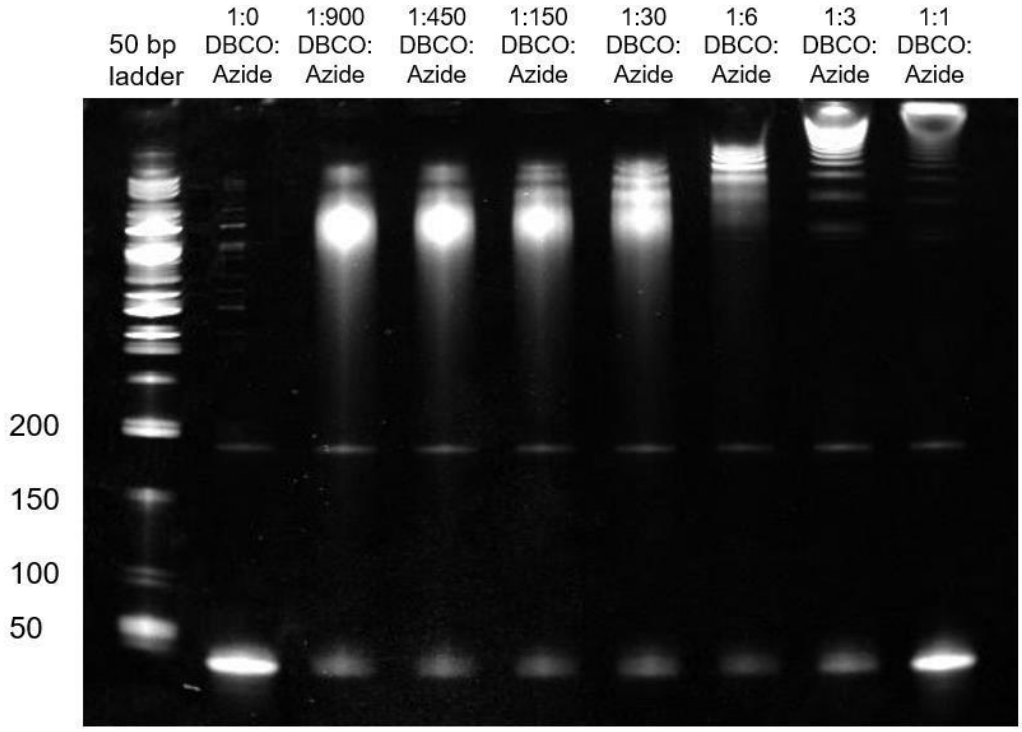

Figure 29. Gel-shift assay to validate conjugation efficiency of various polymer-to-aptamer ratios

A binding study was performed to determine the binding affinity of the aptamer-polymer conjugate (Figure 30). The results revealed that significantly reduced binding affinity (KD ≃ 80nM) compared to unconjugated aptamer (KD ≃ 4nM). However, this is likely due to the substantially larger size of the multivalent aptamer-polymer conjugate, which if fully exists in a

5:1 aptamer to polymer ratio, has a molecular weight of 106 kD. Although binding is reduced, the added bulk to the aptamer should theoretically improve in vivo circulation half-life. However, whether this truly occurs remains to be investigated.

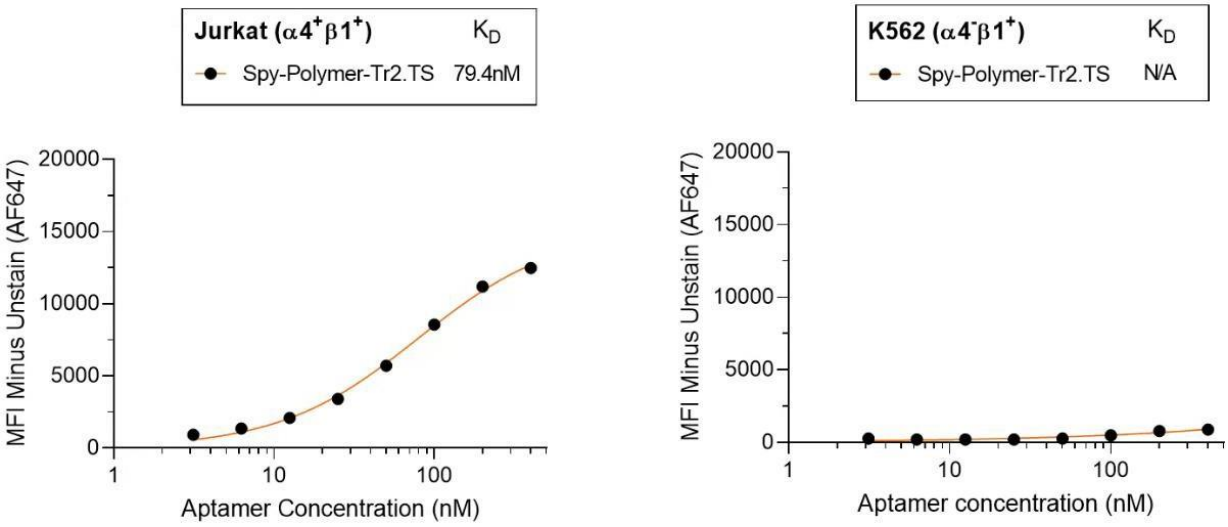

Figure 30. Binding curve of 5:1 HPMA-AzP3MA polymer to DBCO-HR7A1 Trunc2 TS aptamer

Conclusion and Future Directions

The rapid increase in FDA-approved targeted therapies over the last decade represent an industry-wide transition towards precision medicine. Specifically, targeted therapies for oncology indications have been a hotbed of innovation. However, as innovation flourishes, it is important to maintain accessibility of treatment to as many patients as possible. As the average cost of treatment for revolutionary new therapies rises every year, more treatments are becoming increasingly out-of-reach for the average individual. Most current targeted therapies depend on the specificity of monoclonal antibodies for their target receptor. Although effective, monoclonal antibodies are expensive to produce due to their biological synthesis process and extensive and labor-intensive purification procedures. Antibodies also have limited shelf-life and are not suited to a wide variety of chemical modifications. Additionally, antibodies exhibit high variability between batches, with

significant differences in binding observed between antibodies that marketed as binding the same receptor.

In this therapeutic landscape, DNA aptamers present a unique opportunity to improve the effectiveness and availability of targeted treatments. As synthetic polymers, aptamers are inexpensive to produce and can be easily modified to incorporate unique moieties. Aptamers also demonstrate receptor-specificity with affinities similar to antibodies in the pM-nM range, while exhibiting little immunogenicity and a near-unlimited shelf-life. However, aptamers carry a few notable flaws that prevent their immediate translation from bench to bedside. As oligonucleotide sequences, aptamers are targeted by nucleases in blood serum, which often results in swift degradation before reaching the antigen target. Additionally, although the covalent bonds in aptamers are stable at high temperatures, the electrostatic interactions that form the 3D structures and binding moieties of the aptamer behave differently at 37C compared to 4C. Lastly, due to their small size, unmodified aptamers have low circulation half-lives and are rapidly filtered by the kidneys.

The findings from this project have revealed characteristics of the HR7A1 aptamer, and aptamers at-large, that will better inform the further development of a robust aptamer-driven cancer targeting system. A high-affinity, cancer-selective aptamer was extensively characterized through numerous assays, and a comprehensive binding profile was constructed. Thermal stability improvements to the aptamer were also made using modifications informed by predictive modeling software; this resulted in increased 37C binding compared to unmodified aptamer. However, this project also revealed some of the limitations of structural modeling in predicting in vitro and in vivo characteristics of aptamers. Lastly, the HR7A1 aptamer was successfully

conjugated to a high molecular weight polymer using Cu-free click chemistry to potentially improve the in vivo pharmacokinetics of the aptamer.

Future work should continue to focus on improving the circulation time of aptamers in vivo. While this project focused on characterization, serum stability, and thermal stability, circulation time is arguably the most potent limiting factor of aptamer success in vivo. Glomerular filtration rates have been shown to demonstrate charge-selective as well as size-selective properties, due to the electrostatic charge present on the glomerular filtration barrier [22]. Therefore, efforts to mitigate this filtration could focus on either or both aspects, increasing the size of the aptamer via bulky conjugates, or changing the overall molecular charge to stymie the electrostatically driven filtration at the glomerular barrier. Due to the wide array of possibilities for aptamer application beyond this project, the discovery and detailed characterization of the aptamer of a high-affinity, cancer selective aptamer lays the groundwork for further study and application of this aptamer by the lab.

Methods

I. Aptamer-Antibody Co-Staining

Six staining solutions were prepared: control aptamer (10nM Cy5 tJBA), test aptamer, (10nM Cy5 HR7A1), antibody single stains (20nM CD49d FITC and 20nM CD29 PE), control combination (10nM Cy5 tJBA + 20nM CD49d FITC + 20nM CD29 PE), and test combination (10nM Cy5 HR7A1 + 20nM CD49d FITC + 20nM CD29 PE). 100uL of each staining solution was added to wells containing either 0.2E+6 of Jurkat (CD49d+, CD29+), H9 (CD49d+, CD29+), or K562 (CD49d-, CD29+), cells stained with Zombie Violet. Incubation was performed at 4C for 30 minutes. Cells were then washed twice with 200uL wash buffer (WB: 500mL DPBS, Calcium, Magnesium + 2.25g glucose + 2.5mL 1M MgCl2) 1% BSA and fixed with WB 1% BSA + 0.1% PFA before being analyzed on an Attune NxT flow cytometer.

II. Antibody-Antibody Co-staining

Three staining solutions were prepared: two antibody single stains (20nM CD49d FITC and 20nM CD29 PE) and one full stain (20nM CD49d FITC + 20nM CD29 PE). 100uL staining solution was added to wells containing 0.2E+6 of Jurkat, H9, or K562 cells and cells were incubated at 4C for 30 minutes. Cells were then washed twice with 200uL WB 1% BSA and fixed with WB 1% BSA + 0.1% PFA before analysis via flow cytometry.

III. CD29 siRNA Knockdown

To ensure cells were in exponential growth at the time of nucleofection, Jurkat cells were seeded at 0.2E+6/mL 48 hours prior. 100pmol of control siRNA (DS NC1) and CD29 siRNA (DsiRNA 1) were supplemented with Cell Line Nucleofector Solution V (Lonza). 2E+6 cells were then added to the nucleofection solution and were nucleofected using Program X-001. Cells were

then immediately resuspended in 500uL pre-warmed media (RPMI + 10% FBS) and transferred to the appropriate well of a pre-warmed 12-well plate. 24 hours post-nucleofection, cells were transferred to a pre-warmed 6-well plate and diluted 1:2. 42 hours post-nucleofection, five staining solutions were made (20nM CD8A3t, 20nM HR7A1 Cy5, 20nM Sgc4f, 1:50 CD49d FITC, 1:50 CD29 PE; 1:100 tRNA) and each added to 0.1E+6 Jurkat cells. After 30 minutes of incubation at 4C, cells were washed twice with WB 1% BSA and fixed with WB 1% BSA + 0.1% PFA before analysis via flow cytometry.

IV. Aptamer Binding Assays

Aptamers were folded at 95C followed by snap cooling at 4C. Serial dilutions (from 0.1562nM, 0.3125nM, 0.39nM, to 20nM, 40nM, 50nM respectively) for fluorophore-tagged aptamers were prepared in a staining solution of WB 1% BSA. 1:100 tRNA was added to discourage non-specific charge-driven binding. Jurkat and K562 cells were plated at 2E+5 per well in a 96-well round bottom plate and stained with Zombie Violet. 100uL of each staining solution was added to each well of 2E+5 cells and incubated for 30 minutes at 4C. Cells were then centrifuged, washed twice with WB 1% BSA, and fixed with WB 1% BSA + 0.1% PFA before analysis via flow cytometry.

V. Aptamer Competition Assays

Aptamers were folded at 95C followed by snap cooling at 4C. 1mL of 2X aptamer solution (40nM) of HR7A1 was prepared. 2X serial dilutions of both Sgf4f and tJBA8.1 (control) were then prepared, ranging from 320nM to 2.5nM with WB 1% BSA and 1:100 tRNA. Appropriate amounts of FAM tJBA8.1 or FAM Sgc4f were added to 40nM HR7A1 in a 1:2 ratio. Staining solutions (containing varying concentrations of Sgc4f or tJBA8.1 and fixed concentrations of 20nM HR7A1)

were added to 0.1E+6 Jurkat cells and incubated for 30 minutes. Cells were then washed with WB 1% BSA, fixed with WB 1% BSA + 0.1% PFA, and run on the cytometer for analysis.

VI. Functional Serum Stability

Normal mouse serum was thawed and placed on ice. 100uL 1uM of each aptamer (Cy5 HR7A1, Trunc1, Trunc2, Sgc4f, Trunc2 2'OMe) was folded at 95C for 5 min then snap cooled at 4C. 5uL 2uM of each aptamer was added to 5uL mouse serum (1uM final) and incubated for the varying times between 0 and 4 hours. After incubation, aptamers were mixed into separate staining solutions (1.1uL 1M aptamer + 108.8uL WB 1% BSA 1:100 tRNA). 100uL of each staining solution was added to wells containing 0.2E+6 Jurkat cells and incubated for 30min at 4oC. After incubation, cells were spun down and washed twice with 200uL WB 1% BSA, fixed with WB 1% BSA 0.1% PFA, and analyzed on the flow cytometer.

VII. Thermal Stability Evaluation

100uL 1uM Cy5 aptamer was folded at 95C for 5 min and snap cooled at 4C. Aptamer staining solutions were prepared at 10uM with WB 1% BSA + 1:100 tRNA. Aptamer staining solutions were placed at either 4C, 20C, or 37C to equilibrate. H9, Jurkat, and K562 cells were stained with Zombie violet and plated at 0.2E+6 per well into three separate 96-well plates. The three plates were then placed in either 4C, 20C, or 37C conditions for 30 minutes to equilibrate. 100uL of each staining solution was added to cells corresponding to equilibrated temperature and left to incubate at the respective temperatures for 30 min. Cells were then centrifuged, washed twice with WB 1% BSA, and fixed with WB 1% BSA + 0.1% PFA before being analyzed on the flow cytometer.

VIII. Thiol-Aptamer Conjugation to DSPE-PEG(2000) Maleimide

Disulfide (S-S) bonds of the thiol-Trunc2TS aptamer were reduced by treatment with an excess TCEP solution, after being heated for 3 min at 70C. Left to incubate for 57 minutes at room temperature while being protected from light. Excess TCEP was removed via a 10K MWCO column and two washings with DPBS 2mM EDTA. Reduced aptamer concentration was measured using the NanoDrop UV-Vis spectrophotometer. DSPE-PEG(2000)-Maleimide was added to buffer-exchanged aptamer at a 100:1 lipid-to-aptamer molar ratio. The conjugation solution was left to incubate overnight on a thermal shaker set to 10C and 500rpm shaking. The conjugation reaction was run on a 15% TBE urea gel and stained in 1X SYBR Gold before being imaged on a Xenogen IVIS Spectrum to evaluate reaction efficiency. Excess DSPE-PEG(2000)-Maleimide was then removed via ethanol precipitation and the conjugated aptamer was dissolved in 50uL sterile wash buffer.

References

1. Deckert P. M. (2009). Current constructs and targets in clinical development for antibody-based cancer therapy. *Current drug targets*, 10(2), 158–175. https://doi.org/10.2174/138945009787354502
2. Bae, Y. H., & Park, K. (2011). Targeted drug delivery to tumors: myths, reality, and possibility. *Journal of controlled release: Official journal of the Controlled Release Society*, 153(3), 198–205. https://doi.org/10.1016/j.jconrel.2011.06.001
3. Wang, S. S., Yan, Y. S., & Ho, K. (2021). US FDA-approved therapeutic antibodies with high-concentration formulation: summaries and perspectives. *Antibody therapeutics*, 4(4), 262–272. https://doi.org/10.1093/abt/tbab027
4. Hernandez, I., Bott, S. W., Patel, A. S., Wolf, C. G., Hospodar, A. R., Sampathkumar, S., & Shrank, W. H. (2018). Pricing of monoclonal antibody therapies: higher if used for cancer? *The American journal of managed care*, 24(2), 109–112.
5. Thiviyanathan, V., & Gorenstein, D. G. (2012). Aptamers and the next generation of diagnostic reagents. *Proteomics*. Clinical applications, 6(11-12), 563–573. https://doi.org/10.1002/prca.201200042
6. Lakhin, A. V., Tarantul, V. Z., & Gening, L. V. (2013). Aptamers: problems, solutions and prospects. *Acta naturae*, 5(4), 34–43.
7. Ni, S., Yao, H., Wang, L., Lu, J., Jiang, F., Lu, A., & Zhang, G. (2017). Chemical Modifications of Nucleic Acid Aptamers for Therapeutic Purposes. *International journal of molecular sciences*, 18(8), 1683. https://doi.org/10.3390/ijms18081683
8. Zeng, Z., Parekh, P., Li, Z., Shi, Z. Z., Tung, C. H., & Zu, Y. (2014). Specific and sensitive tumor imaging using biostable oligonucleotide aptamer probes. *Theranostics*, 4(9), 945–952. https://doi.org/10.7150/thno.9246
9. Parekh, P., Kamble, S., Zhao, N., Zeng, Z., Portier, B. P., & Zu, Y. (2013). Immunotherapy of CD30-expressing lymphoma using a highly stable ssDNA aptamer. *Biomaterials*, 34(35), 8909–8917. https://doi.org/10.1016/j.biomaterials.2013.07.099
10. Bae, Y. H., & Park, K. (2011). Targeted drug delivery to tumors: myths, reality and possibility. *Journal of controlled release : official journal of the Controlled Release Society*, 153(3), 198–205. https://doi.org/10.1016/j.jconrel.2011.06.001
11. Guo P. (2010). The emerging field of RNA nanotechnology. Nature nanotechnology, 5(12), 833–842. https://doi.org/10.1038/nnano.2010.231
12. Zhou, J., & Rossi, J. (2017). Aptamers as targeted therapeutics: current potential and challenges. Nature reviews. *Drug discovery*, 16(3), 181–202. https://doi.org/10.1038/nrd.2016.199
13. Drolet, D. W., Nelson, J., Tucker, C. E., Zack, P. M., Nixon, K., Bolin, R., Judkins, M. B., Farmer, J. A., Wolf, J. L., Gill, S. C., & Bendele, R. A. (2000). Pharmacokinetics and safety of an anti-vascular endothelial growth factor aptamer (NX1838) following injection into the vitreous humor of rhesus monkeys. *Pharmaceutical research*, 17(12), 1503–1510. https://doi.org/10.1023/a:1007657109012
14. Ruggiero, A., Villa, C. H., Bander, E., Rey, D. A., Bergkvist, M., Batt, C. A., Manova-Todorova, K., Deen, W. M., Scheinberg, D. A., & McDevitt, M. R. (2010). Paradoxical

glomerular filtration of carbon nanotubes. *Proceedings of the National Academy of Sciences of the United States of America*, 107(27), 12369–12374. https://doi.org/10.1073/pnas.0913667107

15. Chigaev, A., Wu, Y., Williams, D. B., Smagley, Y., & Sklar, L. A. (2011). Discovery of very late antigen-4 (VLA-4, alpha4beta1 integrin) allosteric antagonists. *The Journal of biological chemistry*, 286(7), 5455–5463. https://doi.org/10.1074/jbc.M110.162636
16. Berrazouane, S., Doucet, A., Boisvert, M., Barabé, F., & Aoudjit, F. (2021). VLA-4 Induces Chemoresistance of T Cell Acute Lymphoblastic Leukemia Cells via PYK2-*Mediated Drug Efflux. Cancers*, 13(14), 3512. https://doi.org/10.3390/cancers13143512
17. Lyu, Y., Chen, G., Shangguan, D., Zhang, L., Wan, S., Wu, Y., Zhang, H., Duan, L., Liu, C., You, M., Wang, J., & Tan, W. (2016). Generating Cell Targeting Aptamers for Nanotheranostics Using Cell-SELEX. *Theranostics*, 6(9), 1440–1452. https://doi.org/10.7150/thno.15666
18. Xu, J.; Craig, S. L. Thermodynamics of DNA Hybridization on Gold Nanoparticles. *J. Am. Chem. Soc.* 2005, 127 (38), 13227– 13231, https://doi.org/10.1021/ja052352h
19. Jawalekar, Anup M et al. "Oligonucleotide tagging for copper-free click conjugation." *Molecules* (Basel, Switzerland) vol. 18,7 7346-63. 24 Jun. 2013, https://doi.org/10.3390/molecules18077346
20. Seela, Frank, and Suresh S Pujari. "Azide-alkyne "click" conjugation of 8-aza-7-deazaadenine-DNA: synthesis, duplex stability, and fluorogenic dye labeling." *Bioconjugate chemistry* vol. 21,9 (2010): 1629-41. https://doi.org/10.1021/bc100090y
21. Hong, V., Steinmetz, N. F., Manchester, M., & Finn, M. G. (2010). Labeling live cells by copper-catalyzed alkyne--azide click chemistry. *Bioconjugate chemistry*, 21(10), 1912–1916. https://doi.org/10.1021/bc100272z
22. Hausmann, R., Kuppe, C., Egger, H., Schweda, F., Knecht, V., Elger, M., Menzel, S., Somers, D., Braun, G., Fuss, A., Uhlig, S., Kriz, W., Tanner, G., Floege, J., & Moeller, M. J. (2010). Electrical forces determine glomerular permeability. *Journal of the American Society of Nephrology*: JASN, 21(12), 2053–2058. https://doi.org/10.1681/ASN.2010030303

Acknowledgements

I would like to thank Dr. Pun for allowing me to pursue this project in her lab. Having joined this group almost five years ago as an undergraduate freshman, my experience at the University of Washington has been indelibly shaped by my experiences in the Pun Laboratory.

Through Dr. Pun's careful guidance, I have been able to complete both my undergraduate capstone and master's thesis in a field that I am very passionate about. I am also grateful to have had the opportunity to interact with countless brilliant and supportive scientists in the Pun Laboratory, whose unending support and constant encouragement kept me optimistic even when things don't go according to plan.

I am incredibly grateful to Ian Cardle, my graduate student mentor, for his limitless patience in guiding me through every facet of this project. The impact of his continual guidance and scientific expertise cannot be understated and will be dearly missed as I move on from the lab

Thank you to Dr. Kueh for serving on my thesis defense committee, and for furthering my love for immunology through his bioengineering courses. Lastly, I want to thank the Mary Gates Research Endowment for Students for their scholarship support of this research.

Appendix

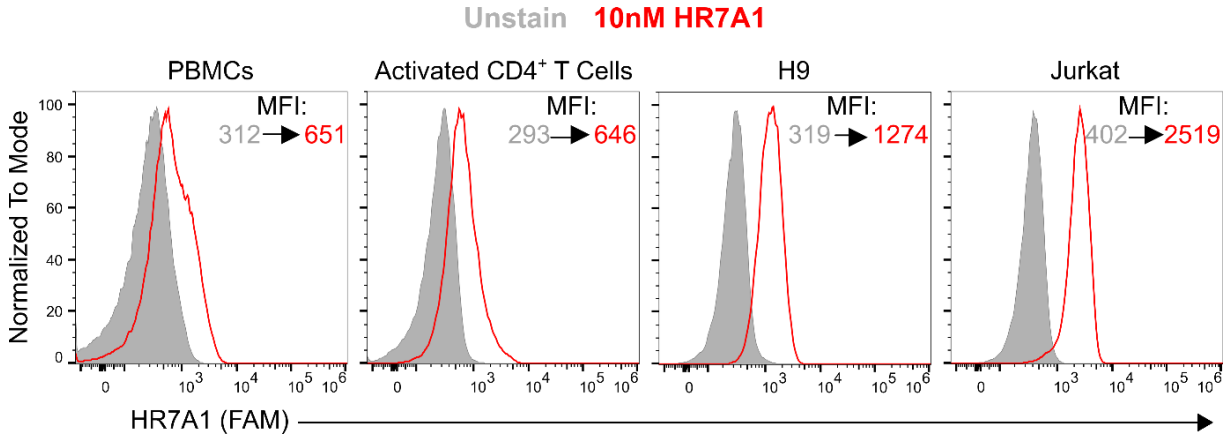

Figure S1. HR7A1 binding to four different cell populations (PBMCs, Activated CD4+ T cells, H9 cells, and Jurkat cells). X-axis displays the mean fluorescence intensity (MFI) of either unstained cells (gray) or cells incubated with 10nM HR7A1 (red).